Germ layer patterning via morphogen crosstalk

Dissertation

der Mathematisch-Naturwissenschaftlichen Fakultät

der Eberhard Karls Universität Tübingen

zur Erlangung des Grades eines

Doktors der Naturwissenschaften

(Dr. rer. nat.)

vorgelegt von

GARY HUI MING SOH

aus Singapur/Singapur

Tübingen

2020

Gedruckt mit Genehmigung der Mathematisch-Naturwissenschaftlichen Fakultät der Eberhard Karls Universität Tübingen.

Tag der mündlichen Qualifikation:	30.09.2020
Stellvertretender Dekan:	Prof. Dr. József Fortágh
1. Berichterstatter:	Prof. Dr. Patrick Müller
2. Berichterstatter:	Prof. Dr. Robert Feil

Acknowledgments

Firstly, I would like to give my utmost gratitude to Prof. Dr. Patrick Müller for supervising my PhD project, as well as his guidance and mentorship for without which the thesis would not have been possible.

I would also like to express my gratitude to my colleagues and friends from the Müller Lab for their direct input in this thesis. Autumn Penecilla Pomreinke for helping with some experiments on my paper, Dr. Katherine W. Rogers for provision of many scientific reagents and helping review my manuscript, Dr. Daniel Čapek and David Mörsdorf for feedback on my manuscript, and Dr. María Almuedo-Castillo for teaching me how to carry out fluorescence *in situ* hybridization. I also thank all lab members in the Müller Lab, both past and present, that I had the pleasure of working with.

I would also like to thank all the technical personnel in the lab, namely Maria Langegger, Christine Henzler, Catrin Weiler and Sarah Keim, for maintaining the regular functions of the lab. I am also grateful to Dieter Labusch for taking care of the fish stocks in the lab.

I further thank Prof. Dr. Robert Feil and Prof. Dr. Frank Chan, who helped me as part of my thesis advisory committee.

Lastly, I would like to thank the Max Planck Society and the German taxpayers for funding this project.

This page intentionally left blank

Contents

This page intentionally left blank

List of figures

List of abbreviations

ADMP	Antidorsalizing morphogenetic protein
BMP	Bone morphogenetic protein
Cas9	CRISPR-associated 9
CRISPR	Clustered, regularly interspaced, short palindromic repeats
DNA	Deoxyribonucleic acid
Dpp	Decapentaplegic
EGF-CFC	Epidermal growth factor-Cripto, FRL-1, and Cryptic motif
Eve1	Even-skipped-like1
FCS	Fluorescence correlation spectroscopy
FDAP	Fluorescence decay after photoconversion
FGF	Fibroblast growth factor
FISH	Fluorescence in situ hybridization
Foxi1	Forkhead box I1
FRAP	Fluorescence recovery after photobleaching
Gdf3	Growth and differentiation factor 3
GFP	Green fluorescent protein
Gsc	Goosecoid
iFRAP	Inverse Fluorescence recovery after photobleaching
mRNA	Messenger RNA
mVenus	Monomeric Venus
Oep	One-eyed pinhead
pSmad	Phosphorylated Smad
sfGFP	Superfolder green fluorescent protein
Shh	Sonic hedgehog
Sog	Short gastrulation
Smad	Combination of *C. elegans* SMA ("small") and *Drosophila* MAD ("Mothers against decapentaplegic")
TALEN	Transcription activator-like effector nucleases
TGF-β	Transforming growth factor - beta
Wnt	Combination of *Drosophila* Wingless and mouse Int-1
WT	Wild type

1. Summary

During early embryonic development, the naïve undifferentiated cells of the early blastula must be specified correctly in accordance with the organism's body plan. This process is mediated in part by secreted signaling molecules called 'morphogens', which diffuse from a localized source and form a concentration gradient across the tissue. This concentration gradient generates a signaling gradient, and cells then respond differently to different levels of the graded signal. Via morphogens, the one-dimensional information encoded in the DNA strands is transformed into a three-dimensional coordinate system that direct the formation of appropriate cell fates at the correct location in the embryo. However, the mechanisms by which a morphogen forms a gradient and the means by which they signal is still highly contentious and under active research.

Nodal and BMP are two such morphogens studied in this dissertation. As they control the critical processes of zebrafish early embryonic development, they have received both intensive research as well as conflicting conclusions. Nodal and BMP are secreted TGF-β proteins that bind to transmembrane serine/threonine kinase receptors, which then phosphorylate their respective Smad proteins (Smad2/3 for Nodal, and Smad1/5/8 for BMP). Nodal plays a key role in germ layer patterning, while BMP controls dorsal-ventral patterning. Together, their mutual interaction triggers the signaling pathways needed to build an embryonic axes. This was strikingly shown when ectopically expressed sources of Nodal and BMP lead to the generation of a secondary embryonic axis. However, how the Nodal and BMP gradients form and how their signaling processes are regulated has become controversial as of late. Although the Nodal signaling gradient was previously found to spread via diffusion, later results contradicts this view and suggest that Nodal signaling is instead formed by an auto-induction relay mechanism. Similarly, recent results suggest that the BMP signaling gradient is the result of a BMP mRNA expression gradient, questioning the role of diffusion in its gradient formation. This contradicts previous results in other model organisms that show that BMP diffusion is important in the formation of its signaling gradient. Hence, this dissertation aims to generate new tools to assist our study of morphogens, as well as apply them to understand the behavior of Nodal and BMP to resolve the current controversy.

In order to achieve this, I developed a simple and effective transplantation device which can be used to transplant cells from one embryo to another to generate a localized morphogen

source which I used to study how the morphogen gradient forms and how it induces signaling. To study the resultant signaling, I additionally developed a protocol to stain both pSmad2/3 and pSmad1/5/8 simultaneously, as well as an optimized workflow to generate two-dimensional cartographical projections of zebrafish embryos for analysis of pSmad staining. I further developed an *in vitro* system to benchmark new software for the analysis of fluorescence recovery after photobleaching assays (which are used to measure diffusion coefficients).

Utilizing the tools I developed, I measured the biophysical properties of fluorescently tagged BMP2b in zebrafish embryos, and found that it diffuses and rapidly forms an extracellular protein gradient from a localized source. We also found that the BMP signaling gradient is formed via a graded source-sink mechanism with BMP and its inhibitor, Chordin, suggesting that diffusion is important in the formation of the BMP signaling gradient. By transplanting sources of fluorescently tagged Nodal and BMP into zebrafish embryos, I found that they both form similar protein gradients and signal cell non-autonomously, providing evidence that they act as morphogens and that their gradient is formed by diffusion. Intriguingly, I found that the signaling range of Nodal (pSmad2/3) is shorter than that of BMP (pSmad1/5/8). Using mathematical modelling and experimental testing, I show that this is due to Nodal having slow signaling kinetics and BMP having fast signaling kinetics. I also further discovered that different ratios of constitutively active Smad2 and Smad5 can induce different embryonic structures, showing that the embryonic axis inducing properties of Nodal and BMP are directly mediated through their Smads. Strikingly, I found that Smad2 and Smad5 antagonize each other only for specific cell fates and not others, providing an elegant mechanism for how cells integrate different ratios of Nodal and BMP signals during development.

2. Zusammenfassung

Während der embryonalen Frühentwicklung müssen die undifferenzierten Zellen des frühen Blastulastadiums so spezifiziert werden, dass der Organismus seinem Bauplan entsprechend richtig geformt wird. Dieser Prozess wird teilweise durch sezernierte Signalmoleküle, die „Morphogene“ genannt werden, gesteuert. Diese diffundieren ausgehend von produzierenden Zellen und formen einen Konzentrationsgradienten im Gewebe. Dieser Konzentrationsgradient resultiert in einem Signalgradienten und die Zellen reagieren der Morphogenkonzentration entsprechend. Durch Morphogene kann die eindimensionale Information, die in den DNA-Strängen kodiert ist, in ein dreidimensionales Koordinatensystem übersetzt werden, in dem sich alle Zelltypen an den korrekten Positionen im Embryo befinden. Allerdings ist der Mechanismus, durch welchen ein Morphogen einen Gradienten bildet, und die Art der Signalübertragung noch umstritten.

Nodal und BMP sind Beispiele für derartige Morphogene und werden in dieser Dissertation untersucht. Sie regulieren kritische Prozesse während der Frühentwicklung des Zebrafischembryos und sind mit widersprüchlichen Ergebnissen intensiv erforscht worden. Nodal und BMP sind sezernierte TGF-β Proteine, die an Serin/Threonin-Kinaserezeptoren binden, welche dann ihre jeweiligen Smad-Proteine (Smad2/3 im Falle von Nodal, Smad1/5/8 bei BMP) phosphorylieren. Nodal spielt eine Schlüsselrolle in der Keimblattmusterbildung, während BMP die dorsoventrale Musterbildung kontrolliert. Die gegenseitige Wechselwirkung zwischen den beiden aktiviert die Signalwege, die notwendig sind, um die embryonale Körperachse zu bilden. Dieser Effekt tritt beeindruckend zu Tage, wenn ektopische Nodal- und BMP-Quellen zur Entstehung einer zweiten Körperachse führen. Wie die Nodal- und BMP-Gradienten gebildet werden und wie ihre Signalprozesse reguliert werden ist seit einigen Jahren umstritten. Obwohl schon früh gezeigt worden ist, dass Nodal ein Morphogen ist, dessen Signal sich durch Diffusion ausbreitet, widersprechen rezente Ergebnisse dieser Ansicht und legen nahe, dass das Nodalsignal mithilfe von Autoaktivierung von Zelle zu Zelle gestaffelt übertragen wird. In ähnlicher Weise deuten neuere Ergebnisse darauf hin, dass der BMP-Signalgradient durch einen BMP-mRNA-Gradienten entsteht, was die Rolle von Diffusion bei der Gradientenbildung in Frage stellt. Dies widerspricht früheren Ergebnissen in anderen Modellsystemen, nach denen Diffusion für die Bildung des Signalgradienten notwendig ist. Daher ist es das Ziel dieser Dissertation, neue Werkzeuge zu schaffen, die dabei helfen können, das Verhalten von Nodal und BMP zu verstehen, und mithilfe dieser die aktuelle Kontroverse aufzulösen.

Um dies zu erreichen, habe ich ein einfaches und effektives Transplantationsgerät entwickelt, mithilfe dessen Zellen von einem Embryo in einen anderen transplantiert werden können, um eine lokale Morphogenquelle zu schaffen. Diese lokale Morphogenquelle kann dann verwendet werden, um zu untersuchen wie der jeweilige Gradient gebildet wird und wie das Signal entsteht. Ferner habe ich ein Protokoll entwickelt, um gleichzeitig pSmad2/3 und pSmad1/5/8 anzufärben, und einen Arbeitsablauf, um zweidimensionale kartographische Projektionen von Zebrafischembryonen für die Analyse der pSmad-Färbungen herzustellen. Ich habe außerdem ein in-vitro-System etabliert, welches das Benchmarking einer neuen Software für die Analyse von FRAP-Experimenten, die verwendet werden um die Diffusionskoeffizienten von Morphogenen zu bestimmen, ermöglicht.

Unter Anwendung der von mir entwickelten Werkzeuge habe ich die biophysikalischen Eigenschaften von fluoreszenzmarkiertem BMP2b in Zebrafischembryonen gemessen und herausgefunden, dass diese diffundieren und schnell extrazelluläre Proteingradienten bilden. Wir konnten auch zeigen, dass der BMP-Gradient mithilfe eines source-sink-Mechanismus durch BMP und seinem Inhibitor Chordin gebildet wird, was gegen frühere Ergebnisse spricht, die behaupten, dass Diffusion in diesem Kontext keine Rolle spielt. Durch die Transplantation von Zellen, welche fluoreszenzmarkierte Nodals und BMPs exprimieren, fand ich heraus, dass beide ähnliche Gradienten bilden und ihre Signale nicht-autonom auf andere Zellen wirken. Dies impliziert, dass sie als Morphogene agieren und dass ihr Gradient durch Diffusion geformt wird. Interessanterweise ist die Signalreichweite von Nodal (pSmad2/3) kürzer als diejenige von BMP (pSmad1/5/8). Mithilfe eines Mathematischen Model konnte Ich zeigen, dass dies durch eine langsamere Signaltransduktionskinetik von Nodal entsteht. Ich entdeckte ebenso, dass unterschiedliche Verhältnisse von konstitutiv aktivem Smad2 und Smad5 zur Bildung von unterschiedlichen embryonalen Strukturen führen, was zeigt, dass die Fähigkeit von Nodal und BMP eine Körperachse zu induzieren, direkt durch Smads vermittelt wird. Bemerkenswerterweise wirken Smad2 und Smad5 für manche Zellarten entgegengesetzt und für andere nicht, was einen eleganten Mechanismus darstellt, wie Zellen unterschiedliche Anteile von Nodal und BMP Signalen während der Entwicklung integrieren.

3. Publications and author contributions

Pomreinke, A. P., Soh, G. H., Rogers, K. W., Bergmann, J. K., Bläßle, A. J. and Müller, P. (2017). Dynamics of BMP signaling and distribution during zebrafish dorsal-ventral patterning. *eLife* **6**, 25861.

Patrick Müller conceived the study, performed the modeling, and wrote the manuscript with input from all authors. I performed all FRAP and FCS experiments, and made the protocol to streamline the generation of 2D maps. Autumn Pomreinke performed the immunostaining experiments. Alexander Bläßle and Katherine Rogers designed and cloned the Chordin-Dendra2 fusion construct and performed the FDAP experiments. I generated all the remaining fusion constructs together with Katherine Rogers, Autumn Pomreinke, and Jennifer Bergmann. Katherine Rogers conducted all transplantation experiments.

Bläßle, A., Soh, G., Braun, T., Morsdorf, D., Preiss, H., Jordan, B. M. and Muller, P. (2018). Quantitative diffusion measurements using the open-source software PyFRAP. *Nature Communications* **9**, 1582.

The study was conceived by Patrick Müller, Ben Jordan and Alexander Bläßle. I provided most of the FRAP datasets for the study and tested the PyFRAP software before publication. Theresa Braun and Hannes Preiß provided the remaining FRAP datasets. Additionally, I provided feedback on the manuscript. Data analysis was performed by Patrick Müller and Alexander Bläßle.

Soh, G. H., Müller, P. (2018). FRAP analysis of Extracellular Diffusion in Zebrafish Embryos. *Methods in Molecular Biology* **1863**, 107-124.

Patrick Müller and I initiated and outlined the project. I wrote a first draft of the manuscript and performed all experiments and made all the figures. The manuscript was revised with the help of Patrick Müller. I analyzed the results together with Patrick Müller.

Almuedo-Castillo, M., Bläßle, A., Mörsdorf, D., Marcon, L., Soh, G. H., Rogers, K. W., Schier, A. F. and Müller, P. (2018). Scale-invariant patterning by size-dependent inhibition of Nodal signalling. *Nature Cell Biology* **20**, 1032-1042.

The study was conceived by Patrick Müller, Alexander Schier and María Almuedo-Castillo. The experiments were performed by María Almuedo-Castillo, David Mörsdorf and myself. Katherine Rogers generated the *lefty* mutant zebrafish used. Specifically, I designed the device for extirpation of embryos and helped with some of the fluorescence in situ hybridization staining. The results were analyzed by Alexander Bläßle, Luciano Marcon and Patrick Müller. María Almuedo-Castillo and Patrick Müller wrote the manuscript.

Soh, G. H., Pomreinke, A. P., Müller, P. (2020). Integration of Nodal and BMP signaling by mutual signaling effector antagonism. *Cell Reports* **31**, 107487.

I initiated and outlined the project together with Patrick Müller. I wrote the manuscript and performed most of the experiments. Autumn Pomreinke contributed the Western blot and phenotypic analysis of the fluorescent constructs. The mathematical modeling was done by Patrick Müller. The manuscript was revised with the help of Patrick Müller. I analyzed the results together with Patrick Müller.

4. Introduction

4.1 Morphogens and patterning

During development, an embryo consisting of naïve, undifferentiated cells is transformed into an organism made of differentiated cells. In order to achieve this, cells need to know their location within the embryo so that they can differentiate into the right cell types at the right place. To do this, the embryo has to utilize the genetic information contained in its cells to generate the spatial information for constructing the body. An explanation for how this could be achieved is through the use of 'morphogens'. The term was first coined and introduced by Alan Turing when he provided a mathematical model which posited the existence of diffusible substances that can interact with each other to specify different patterns (Turing, 1952). This idea was further extended by Lewis Wolpert in a framework that is now referred to as the 'French flag model' (Wolpert, 1969). In this model, morphogens are molecules that diffuse from a localized source and form a concentration gradient across the tissue (Figure 1). The concentration gradient of the morphogen is converted into a gradient of signaling activity, and the cells then differentiate into various fates in accordance to the level of morphogen signaling activity they are exposed to. This allows morphogens to generate a coordinate system which specifies the appropriate cell fates at the correct location in the embryo, converting the one-dimensional information encoded within DNA into a three-dimensional blueprint.

The existence of secreted signaling factors that direct development was first posited based on the discovery that a section of an embryo, called the organizer, can induce the surrounding naïve cells to form a secondary axis when transplanted into another embryo (Spemann and Mangold, 1924). However, the first signaling factor that can be definitively called a morphogen was only successfully identified much later (Driever and Nüsslein-Volhard, 1988). That morphogen is a transcription factor named Bicoid, which forms an anterior to posterior gradient in the *Drosophila* embryo. It was discovered that changing the Bicoid gradient by increasing or decreasing *bicoid* mRNA expression caused a concomitant shift in the specified cell fates. Thus, it fulfills the conditions of being a morphogen: it forms a gradient, and it induces different cell fates at different levels. Since then, other signaling factors have been shown to function as morphogens, such as Decapentaplegic (Dpp) during *Drosophila* dorsal-ventral layer patterning (Ferguson and Anderson, 1992) and wing formation (Lecuit et al., 1996; Nellen et al., 1996), Sonic Hedgehog (Shh) during vertebrate

neural tube patterning (Briscoe et al., 2001), Activin during *Xenopus* germ-layer patterning (Green et al., 1992; Green and Smith, 1990; Gurdon et al., 1994) and Squint during zebrafish germ-layer patterning (Chen and Schier, 2001).

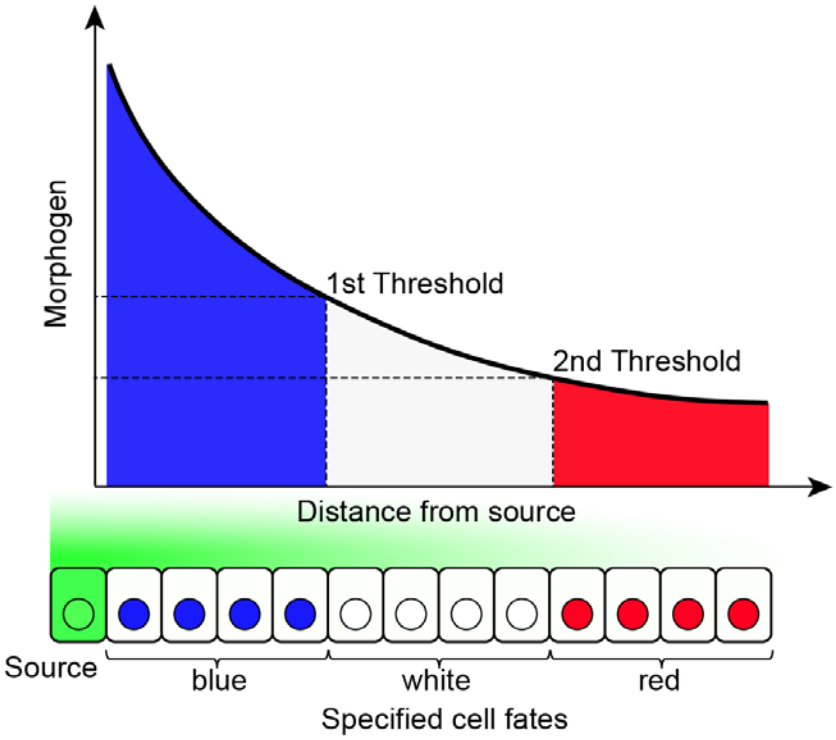

Figure 1: Diagram of the French flag model. In this model, the cells have the potential to assume one of several differentiated fates, denoted as blue, white, or red, based on the concentration of morphogen they are exposed to. High concentrations of morphogens cause them to become blue, while concentration in between the 1st and 2nd threshold makes them white, and concentration below the 2nd threshold makes them red. A source secretes the morphogen which then diffuses across the cells, forming a concentration gradient. Each cell then reads out the morphogen concentration and differentiates into a specific cell fate. This allows morphogens to convey positional information as the cells differentiates into different fates based on their distance from the morphogen source.

The current default model for gradient formation is the 'synthesis-diffusion-clearance model' (Rogers and Schier, 2011). The model was first conceived as the 'source-sink model', in which a localized 'source' produces morphogens which then diffuse across the tissue before they are degraded by 'sink' cells that are located at the opposite end of the source (Crick, 1970). This degradation allows the formation of the gradient by preventing the source from saturating the tissue with morphogens. Later research suggests that instead of a specified 'sink' at the end, morphogens are removed at a constant rate throughout the entire tissue through various mechanisms, such as degradation by endocytosis (Marois et al., 2006; Scholpp and Brand, 2004). However, there has been skepticism that diffusion alone is sufficient in morphogen gradient formation (Kerszberg and Wolpert, 2007). Hence, other

means of gradient formation have been proposed, such as transcytosis (Bollenbach et al., 2007) or filopodia-like projections known as cytonemes (Ramirez-Weber and Kornberg, 1999) that may transport Dpp in *Drosophila* wing disc. However, these posited mechanisms are currently contentious (Müller et al., 2013; Rogers and Müller, 2019). Therefore, in order to understand how morphogen gradients are formed, it is critical to carry out biophysical measurements of both its diffusivity and degradation rate.

Fluorescence recovery after photobleaching (FRAP) and fluorescence correlation spectroscopy (FCS) are two main assays to measure the diffusion coefficient of morphogens directly in living embryos (Müller et al., 2013). FRAP involves photobleaching an area and measuring the fluorescence recovery in this area over time. The recovery curve can then be used to calculate the diffusion coefficient by fitting with an appropriate mathematical model. FCS works by measuring fluorescence fluctuations in a femtoliter volume over a short period of time. An autocorrelation is then performed on the data and it is fitted to the appropriate model to calculate the diffusion coefficient. FCS can also be further extended as two-focus FCS, which can be used to detect active transport in the movement of the morphogens (Dertinger et al., 2007). Due to the difference in scale, FCS measures the 'free diffusivity' while FRAP measures the 'effective diffusivity' which takes into account large scale effects such as tortuosity and transient binding (Müller et al., 2013). Using both of these methods, Fgf8 was shown to be freely diffusing (Yu et al., 2009), supporting the idea that the Fgf8 gradient is generated via the synthesis-diffusion-clearance model (Müller et al., 2013). Currently, the primary method to measure morphogen clearance rates directly in living embryos is via fluorescence decay after photoconversion (FDAP) (Müller et al., 2012; Rogers et al., 2015). FDAP is a form of pulse-chase analysis where the morphogen is tagged with a photoconvertible fluorescent protein. The fluorescence absorption and emission spectra of the photoconvertible protein is then irreversibly changed by strong irradiation with blue light, allowing the user to convert a fixed fraction of protein into a different fluorescence spectrum. Subsequently, the decay of the fluorescence intensity of the photoconverted protein of interest can be measured, and a decay function is fitted to the data to calculate the half-life of the protein.

The ability for different levels of morphogen activity to specify different cell fates is mediated through a diverse array of mechanisms. Bicoid, being a transcription factor, does so by binding cooperatively to DNA (Burz and Hanes, 2001). This cooperative binding sharpens the transition between the bound and unbound state, creating a threshold-like transcriptional

response to different concentrations of Bicoid. In the case of Nodal, the cell integrates over both the duration and the intensity of Nodal signaling it was exposed to (Dubrulle et al., 2015). This is achieved through differences in transcriptional kinetics of different Nodal target genes; genes that are slowly transcribed have a shorter range than genes that are rapidly transcribed. Activin, a TGF-β protein related to Nodal, instead exhibits a molecular 'memory' where cells express genes corresponding to the highest concentration of morphogen they have been exposed to (Gurdon et al., 1995). This is done through a long-lived signaling complex that is formed when Activin is bound to its receptor (Dyson and Gurdon, 1998; Jullien and Gurdon, 2005). Shh relies on a complex gene regulatory logic between its target genes to interpret its gradient (Cohen et al., 2013). Shh, which is secreted from the ventral side, converts Gli from its transcriptional repressor form, GliR, into its transcriptional activator form, GliA. Ventrally restricted genes are induced by GliA, while more dorsal genes are restricted by GliR binding. These genes then mutually cross repress each other's expression, creating sharp boundaries between each expression domain. Hence, the interpretation of morphogen gradients is a complex and diverse process. Although it is likely that every morphogen system has its own unique way of signaling interpretation and has to be studied in a case by case basis, it is possible that general fundamental principles underlying developmental processes can be gleaned from such studies.

4.2 Nodal and BMP in zebrafish patterning

Nodal and BMP are two morphogens that are critical in controlling the earliest cell fate decisions during zebrafish embryogenesis (Rogers and Müller, 2019). Nodal and BMP (Figure 2A) are both secreted proteins from the TGF-β superfamily (Wozney et al., 1988; Zhou et al., 1993). Nodal was first identified through forward genetic screens in mice due to its role in the formation of the embryonic node (Zhou et al., 1993), while BMPs were initially identified and isolated for their role in regulating bone formation (Urist, 1965; Wozney et al., 1988) and their role in embryogenesis was only discovered later in *Drosophila* (Gelbart, 1989; Padgett et al., 1987). Both Nodal and BMP signals through a hetero-tetrameric receptor complex consisting of two TGF-β type I and two TGF-β type II serine/threonine kinase receptors (Wrana et al., 1992). Nodal, unique among TGF-β superfamily proteins, additionally requires the EGF-CFC family co-receptor One-eyed pinhead (Oep) (Shen and Schier, 2000). Nodal and BMP signaling then leads to the phosphorylation of their respective effector Smads, which form a heterotrimer with Smad4 and accumulate in the nucleus where

they regulate the expression of target genes (Heldin et al., 1997). Smad1, 5, and 9 are responsive to BMP signaling, but Smad5 is the primary BMP-responsive Smad during zebrafish early development (Hild et al., 1999), while Smad2 and 3 are activated by Nodal signaling, but Smad2 is the primary Nodal-responsive Smad during early embryogenesis (Dubrulle et al., 2015).

In zebrafish, Squint (Erter et al., 1998; Feldman et al., 1998) and Cyclops (Rebagliati et al., 1998; Sampath et al., 1998) are the two Nodal homologs that are involved in germ layer patterning during early embryogenesis (Chen and Schier, 2001). They form a heterodimer with Gdf3 (also known as Vg1) which is ubiquitously produced throughout the embryo from maternally deposited mRNA (Bisgrove et al., 2017; Montague and Schier, 2017; Pelliccia et al., 2017). There are currently more than ten BMPs discovered so far in vertebrates (Ducy and Karsenty, 2000), but in zebrafish the main BMPs involved in early embryogenesis are Bmp2b and Bmp7 (Schmid et al., 2000). These BMPs form functional Bmp2b/7 heterodimers; homodimers of Bmp2b and Bmp7 alone do not elicit signaling (Little and Mullins, 2009).

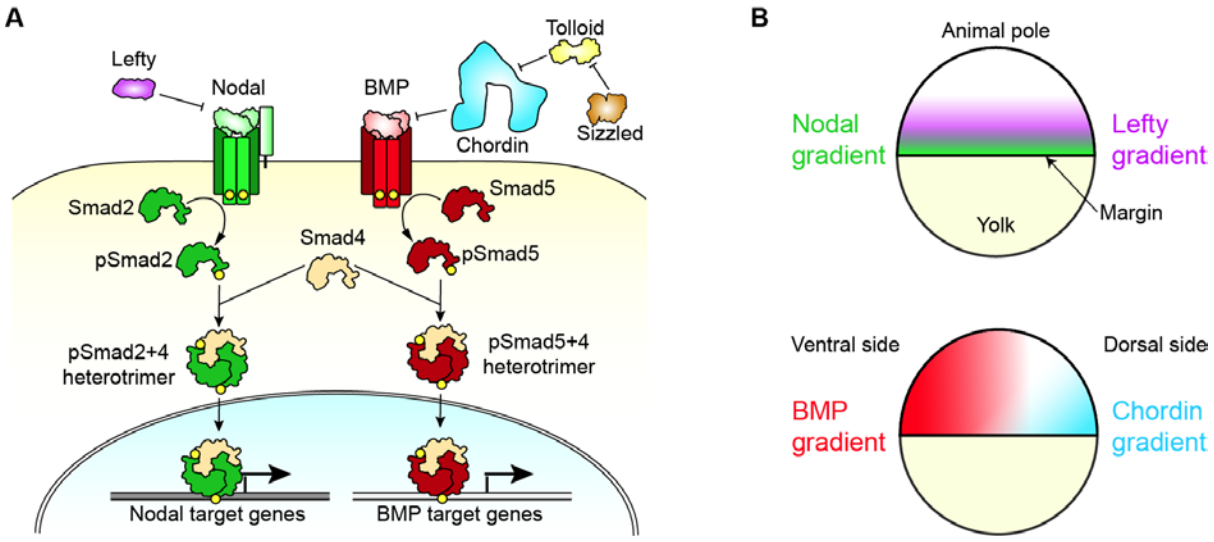

Figure 2: Diagram of the signaling pathway and spatial expression of Nodal and BMP. (A) Binding of Nodal and BMP to their cognate receptors leads to phosphorylation of the type I receptor by the type II receptor. These activated receptors then phosphorylate Smad2 or Smad5 respectively, which forms a heterotrimer with Smad4 and accumulate in the nucleus where they alter the expression of their target genes. Nodal and BMP are regulated by extracellular antagonists such as Lefty and Chordin respectively. Chordin itself is further regulated via proteolytic cleavage by Tolloid, which is in turn inhibited by Sizzled. **(B)** Nodal is expressed along the margin and forms a gradient towards the animal pole. Lefty, being induced by Nodal signaling, is also expressed from the margin towards the animal pole. Its higher diffusivity allows Lefty to form a broader gradient than Nodal. BMP is expressed in a ventral to dorsal gradient, while Chordin is expressed on the dorsal side, close to the margin.

Nodal signaling (Figure 2B) starts from the margin and extends outwards into the overlying cells over time, specifying the naïve cells (which would otherwise become ectoderm) to become mesoderm and endoderm (Feldman et al., 1998). Fgf8 is induced downstream of Nodal signaling, and its longer signaling range helps to extend mesoderm specification farther towards the animal pole (Mathieu et al., 2004; Rodaway et al., 1999; van Boxtel et al., 2015; van Boxtel et al., 2018). BMP signaling (Figure 2B) controls dorsal-ventral patterning and initially starts off weakly throughout the entire embryo, but gradually becomes stronger but restricted to the ventral half (Ramel and Hill, 2013). Wnt8a, which is then induced by combined BMP and Nodal signaling, acts in conjunction with BMP to maintain ventral mesoderm and suppress dorsal mesoderm (Ramel et al., 2005; Ramel and Lekven, 2004).

Nodal and BMPs are both directly inhibited by the extracellular factors Lefty and Chordin respectively. The Lefty proteins, Lefty1 and Lefty2, are both TGF-β proteins like Nodal and are induced by Nodal signaling and function as feedback inhibitors of Nodal (Meno et al., 1999). Chordin, on the other hand, is unrelated to TGF-β proteins and is expressed on the opposite side (the dorsal side) of where BMP is expressed as its transcription is inhibited by BMP signaling (Miller-Bertoglio et al., 1997). Chordin is also further regulated by the extracellular proteins Tolloid and Sizzled. Tolloid is a metalloprotease that inhibits Chordin by cleaving it, leading to enhanced BMP signaling (Blader et al., 1997), while Sizzled binds and inhibits Tolloid, resulting in the suppression of BMP signaling (Muraoka et al., 2006).

Nodal and BMP signaling together were also found to be sufficient to trigger all processes needed to form an embryonic axis. This was strikingly demonstrated when ectopic juxtaposed sources of Nodal and BMP was capable of inducing a secondary embryonic axis (Xu et al., 2014). The ratio of Nodal to BMP signaling was found to be the determining factor in specifying the necessary cell fates for the embryonic axis (Fauny et al., 2009): Nodal by itself creates axial structures, high Nodal to BMP ratios induce posterior head structures, intermediate ratios generate the middle trunk, and low Nodal to BMP ratios organize the tail.

Currently, the signaling and biophysical characteristics of Nodals are better understood compared to BMP. Squint was found to behave as a morphogen as it can act directly at a distance and induce distinct cellular responses in a concentration-dependent manner (Figure 3A), while Cyclops had too short of a signaling range to be considered a morphogen (Chen and Schier, 2001). The morphogenic property of Nodal to induce different cell fates at

different ranges was later shown to be mediated through differences in the kinetics of target gene induction, where genes with higher transcription rates and earlier onset of induction will have a longer expression range (Dubrulle et al., 2015). The diffusion coefficients of fluorescently-tagged Squint and Cyclops, as well as their inhibitors Lefty1 and Lefty2, were also measured and found to be 0.7 $\mu m^2/s$ for Cyclops-GFP, 3.2 $\mu m^2/s$ for Squint-GFP, 11.1 $\mu m^2/s$ for Lefty1-GFP, and 18.9 $\mu m^2/s$ for Lefty2-GFP (Müller et al., 2012). This led to the idea that the fast diffusing Lefty forms a reaction-diffusion system with the slower diffusing Nodal (Müller et al., 2012).

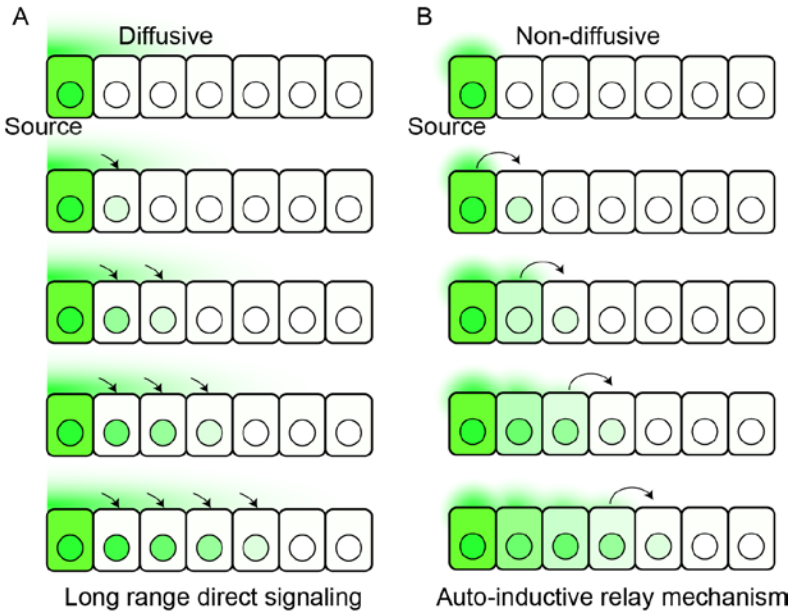

Figure 3: Signaling spread by an auto-inductive relay mechanism compared with long range direct signaling. (A) In the case of long range direct signaling, the signaling molecule diffuses outwards from the source and directly induces signaling in distant cells. **(B)** In an auto-inductive relay mechanism, the poorly diffusive signaling molecule secreted by the source activates signaling only in adjacent cells, which subsequently auto-induces its own production. These cells produce more of these signaling molecules which then auto-induces its own production in neighboring cells, and so on. This allows a poorly diffusive signaling molecule to form a long range signaling gradient.

However, this picture has been complicated by other findings. Recent results show that the mesoderm-inducing ability of Nodal is in part due to FGF signaling (Rodaway et al., 1999; van Boxtel et al., 2015; van Boxtel et al., 2018). Nodal signaling was found to induce the expression of FGF (which has a longer signaling range than Nodal), which then induces mesodermal gene expression at a longer range than Nodal signaling alone. This calls into question earlier results where mesodermal gene induction was used as a readout of Nodal signaling (Chen and Schier, 2001). There are also results suggesting that Nodal forms a relay system with itself (Figure 3B) as Nodal signaling auto-induces the production of more Nodal,

and this interpretation is supported by the discovery that Nodal signaling activity appears to be restricted to regions of Nodal gene expression (van Boxtel et al., 2015). This means that juxtacrine signaling is sufficient for Nodal signaling to spread outwards from the margin, challenging the idea that Nodal needs to diffuse for the spread of Nodal signaling (Figure 3A). The possibility that Nodal does not signal at a distance also throws into doubt the idea that Nodal and Lefty could act as a reaction-diffusion system. Instead, the latter research posits that a transcriptional delay of Lefty induction caused by the microRNA, *miR-430*, is the means by which Lefty restricts the signaling range of Nodal (van Boxtel et al., 2015). Hence, the debate is still ongoing despite all the information acquired about the signaling properties of Nodal.

Before I started on my PhD work, less was known about the signaling and biophysical properties of zebrafish BMP/Chordin system compared to Nodal/Lefty system. Their diffusion coefficient (if they even diffuse) has not been measured, and it is unclear whether they can signal directly at a distance. Work done with BMP homologs in other animals, such as Dpp in *Drosophila*, showed that it behaves as a morphogen during dorsal-ventral patterning (Ferguson and Anderson, 1992). Current work in zebrafish instead suggests that the BMP activity gradient is due to a gradient in the expression profile of BMP, implying that diffusion of BMP is not needed (Ramel and Hill, 2013). At the time, no work had been done to test whether BMP can signal directly at a distance, or whether it can induce different cell fates at different ranges. Thus, it remained uncertain whether BMP can diffuse or signal directly.

The mode of interaction between BMP and its inhibitor Chordin is still hotly debated as well, with the most prominent model being the ‘Shuttling model’. The Shuttling model was originally developed from studies in *Drosophila*, with the BMP homolog Dpp, and the Chordin homolog Sog (Holley et al., 1996; Mizutani et al., 2005; Wang and Ferguson, 2005). Just like in zebrafish, Dpp and Sog are expressed on opposite sides of the embryo, but Dpp is instead expressed on the dorsal side while Sog is expressed on the ventral side. This model proposes that the binding of Sog to immobilized Dpp frees Dpp from its binding to cell surface collagen. This allows the Dpp-Sog complex to diffuse and move to the dorsal side where the Tolloid protease is expressed. Tolloid cleaves Sog and releases Dpp from the Dpp-Sog complex where it then reassociates with collagen and becomes immobile again. This process essentially causes Dpp to accumulate on the dorsal side. The Shuttling model was

later proposed to occur in *Xenopus* as well (Ben-Zvi et al., 2008). Despite the elegance of the Shuttling model, the key biophysical measurements of the diffusion coefficient of Chordin and BMP which are needed to test the shuttling model in zebrafish had not yet been done. Hence, more work was needed to unravel the interaction between BMP and Chordin in zebrafish.

How Nodal and BMP signaling interact during zebrafish germ layer patterning was even less clear. It was known that BMP antagonizes endoderm formation by Nodal (Poulain et al., 2006) and Nodal induces the production of Chordin, thereby inhibiting BMP (Bennett et al., 2007). However, the mechanism that allows different ratio of Nodal and BMP signaling to induce various ectopic structures was unknown (Fauny et al., 2009), as was the means by which ectopic sources of Nodal and BMP induce formation of secondary embryonic axes (Xu et al., 2014).

4.3 Research aims and summary

In this dissertation, I aimed to fill in the gaps in our understanding of how the Nodal and BMP gradients form and signal, as well as how their signaling pathways interact.

As the first step of this research project, I placed my focus in developing the necessary assays and tools to study these processes. In order to measure morphogen gradient formation, a localized source of morphogen production has to be generated. Previous methods utilized blastomere injection (Chen and Schier, 2001; Fauny et al., 2009; Xu et al., 2014) which lacks precise control over the timing, placement and spacing of morphogen producing sources. Hence, I developed a device to transplant cells from zebrafish embryos overexpressing the morphogen into normal embryos (Section 5.1).

We would also need to be able to measure the direct signaling response to Nodal and BMP in order to verify if they could induce signaling directly. Earlier results with Nodal measured the activation of Nodal target genes induced by the Nodal source to conclude that Squint induces signaling at a distance, a defining trait of a morphogen (Chen and Schier, 2001). This result has been complicated by more recent results suggesting that many Nodal target genes are instead secondarily induced by Nodal-induced FGF (van Boxtel et al., 2015). Hence, direct measurement of pSmad induction is required. Since my goal is to understand how Nodal and BMP signaling interact, we need to be able to measure both pSmad2 and pSmad5 signaling

simultaneously as well. Currently, there are protocols to detect pSmad2 or pSmad5 individually via immunostaining (Ramel and Hill, 2013; van Boxtel et al., 2015), but simultaneous staining is complicated as they use antibodies of the same species. Therefore, I developed a protocol that can simultaneously detect both pSmad2 and pSmad5 using tyramide signal amplification (Toth and Mezey, 2007) (Section 5.2).

In order to quantify the pSmad staining across the embryo, I extended a protocol used previously that 'unwraps' the surface of the embryo and projects them on a 2D surface (Schmid et al., 2013). This method generates cartographical projections, but in a random orientation. I therefore developed a method that uses an open-source software, Hugin, to rotate the projection so that it is oriented consistently for the proper quantification of pSmad distribution (Section 5.2).

Since quantification of the diffusion coefficient is needed to understand morphogen gradient formation, I also worked on methods to further develop FRAP. Calculating the diffusion coefficient from FRAP data depends heavily on the mathematical model used hence new software is continuously released to improve the accuracy of the computation. I developed an *in vitro* FRAP model system using well characterized fluorescent-dextrans of various molecular weights as a means of benchmarking, which helped in the development of the new software, PyFRAP (Bläßle et al., 2018) (Section 5.3).

Having established the experimental methods to measure key biophysical parameters of morphogens, we then used these techniques to further our understanding of Nodal and BMP. Unlike Nodal and Lefty, the diffusion coefficient of BMP and its inhibitor, Chordin, is still undetermined. Hence, we used FRAP to measure the diffusion coefficients of BMP and Chordin and found that they had similar diffusion coefficients when measured separately and when co-expressed, contradicting the Shuttling model which predicts that BMP-Chordin complexes have a higher diffusion coefficient (Section 5.4). Through transplantation experiments, whole embryo pSmad imaging and mathematical modeling, we found evidence which indicates that BMP interacts with Chordin via a source-sink model (Section 5.5) (Pomreinke et al., 2017).

In order to study how Nodal and BMP gradients form and how their signaling interacts, we used the secondary axis formation as a model system as it allows us to use ectopic gradients to cause axis induction, a process that is physiologically relevant (Xu et al., 2014). I used the transplantation device to generate ectopic sources of fluorescently-tagged Nodal and BMP,

imaged them and simultaneously stained for pSmad2/3 and pSmad1/5/8 to study the formation of the protein gradient and its signaling gradient. I discovered that Nodal has a shorter pSmad signaling range than BMP even with similar protein gradient, due to a difference in signaling kinetics (Section 5.6). This shows that signaling kinetics is important in regulating the activity range of signaling molecules in addition to their diffusivity. I also found that both Nodal and BMP form long-range gradients that induce downstream pSmad signaling directly without need of a relay mechanism (Section 5.7). Next, In order to understand how the Smads activated by Nodal and BMP signaling induces axis formation, I developed constitutively active versions of Smad2 and Smad5. I found that different ratios of constitutively active Smad2 and Smad5 can generate different ectopic structures, showing that the organizing ability of varying ratios of Nodal and BMP is mediated by varying ratios of Smad2 and Smad5 (Section 5.8). I discovered that Smad2 and Smad5 mutually antagonize each other in a selective manner for certain cell fates, while acting synergistically for others, which allows cells to respond differently to different ratios of Nodal and BMP. This selective, mutual antagonism may represent a general mechanism for how cells integrate and discriminate between two overlapping signals during development.

5. Results and Discussion

As the Nobel laureate Sydney Brenner famously observed, the progress of science "depends on the interplay of techniques, discoveries, and ideas, probably in that order of decreasing importance (Brenner, 2002)." That is very much the case for biology, and this dissertation is no exception. Hence, I will first present the techniques that were developed, followed by the discoveries that were made.

5.1 Simple and effective transplantation device for studying morphogen signaling

From the classic experiments of Mangold and Spemann who showed the existence of an organizer which is capable of instructing the formations of an embryonic axis (Spemann and Mangold, 1924), transplantation of cells between embryos has become a time-honored technique for studying morphogenic signals in development. Transplantation has been used in zebrafish embryos as a means of generating maternal-zygotic mutants via germ line transplantation (Ciruna et al., 2002), and now I would like to use this method to create localized sources to study morphogen gradient formation

A commonly used setup for transplantation, as described in The Zebrafish Book (Westerfield, 1993), consists of a micrometer drive-controlled Hamilton syringe connected to a micropipette holder through a flexible tubing and a reservoir filled with mineral oil (Figure 4A). Turning the screw moves the plunger inside the syringe, and the pressure generated can be used to suck out cells from one embryo and deposit them into another. However, such a device consists of many parts and is laborious to assemble from scratch. Such devices can be also be purchased as a complete working set, usually sold as a 'Manual Microinjector'. There are several versions sold by companies such as Sutter Instrument, but are expensive and usually cost more than USD$1500. In both the homemade and commercial version, the micropipette is fixed separately from the syringe; hence the manipulation of the needle and the movement of the plunger have to be done separately with different hands, reducing the throughput. Furthermore, they are also troublesome to prepare as it needs to be carefully filled with oil so that bubbles do not form. Therefore, we developed a device that is cheap, easy to assemble and simple to use to overcome this issue.

This device is constructed out of a Luer Tip 25 μL Hamilton syringe, 1700 series, and a microelectrode holder with Luer fitting for a 1.0 mm glass capillary (Figure 4B), which in

total cost less than USD$80. Since it consists of only two parts, it is cheap to purchase and easily assembled by inserting the microelectrode holder into the syringe via the Luer lock fitting (Figure 4C). The device is then directly mounted on a micromanipulator, allowing the user to control the position of the device and the suction without moving their hands away from the micromanipulator. This also conveniently leaves the other hand free to steady the transplantation dish. The device works by direct suction with air and does not need to be filled with mineral oil. Due to the attractive forces between the water and the walls of the glass needle, a large movement in the plunger of the syringe translates to a smaller movement in the water level in the needle. This allows the device to suck out a precise amount of cells and transplant them exactly where it is required (Figure 4D). This device was used as an extirpation device in the publication titled "Scale-invariant patterning by size-dependent inhibition of Nodal signalling" (Appx. 4), to reduce the size of zebrafish embryos, and in the publication titled "Integration of Nodal and BMP signaling by mutual signaling effector antagonism" (Appx. 5), where it was used to transplant clones expressing fluorescently tagged Nodal and BMP into zebrafish embryos.

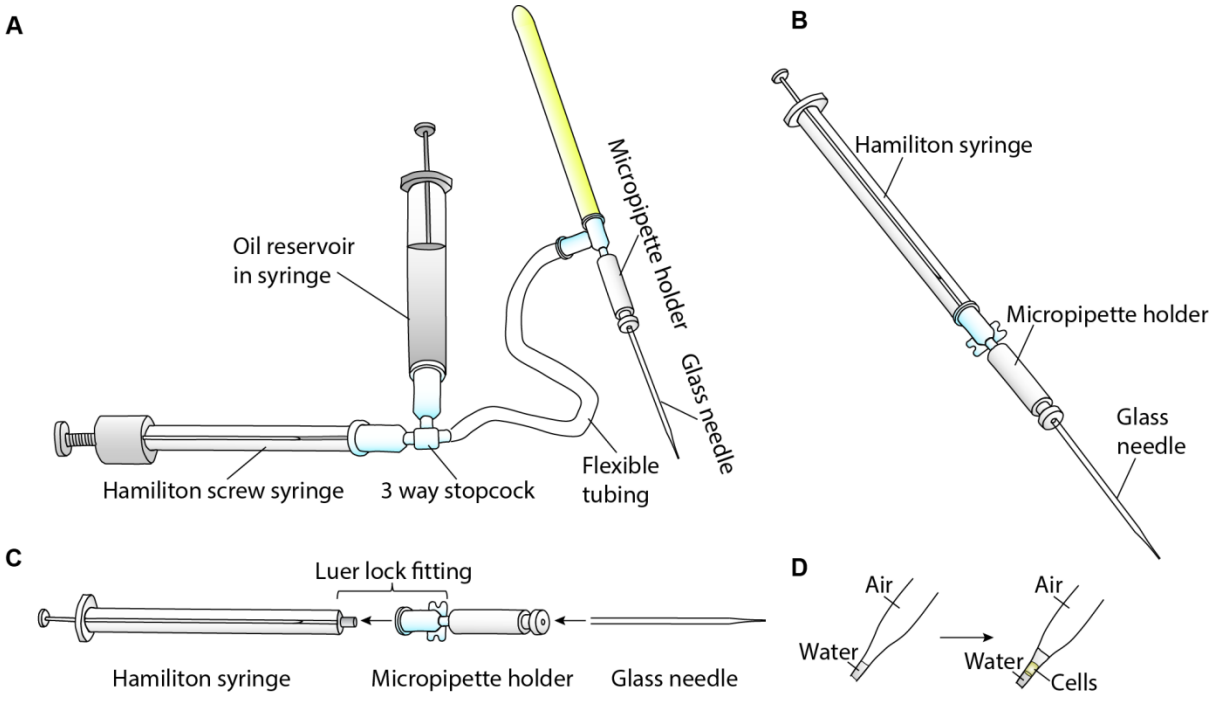

Figure 4: Schematics of transplantation devices. (A) The original transplantation device described in the zebrafish book is a complicated device consisting of a micrometer drive-controlled Hamilton syringe connected to a micropipette holder through a flexible tubing and a reservoir filled with mineral oil. **(B)** The new transplantation device is a simple set up consisting of a Hamilton syringe directly connected to a microelectrode holder, **(C)** which can be fitted together by inserting them directly through the Luer lock fitting**. (D)** By maintaining the water level in the needle at a low level close to the tip, precise control of the suction can be achieved when the plunger is moved.

5.2 Optimization of pSmad immunostaining and visualization

Understanding how Nodal and BMP pattern the zebrafish embryo requires a way to detect their immediate effectors: Smad2 and Smad5. They are activated by phosphorylation on the serine residues in their C-terminal SSXS motif, and are translocated to the nucleus. Hence, we can visualize them by probing with antibodies that specifically bind to the phosphorylated form of the Smads. Antibodies that bind to pSmad2 (van Boxtel et al., 2015) and pSmad5 (Ramel and Hill, 2013) have been used successfully in zebrafish. However, these antibodies are both raised from rabbits and conventionally staining them with fluorescently-labelled anti-rabbit secondary antibodies will cause the detected pSmad2 and pSmad5 signal to overlap. Therefore, a method is needed to ensure that they can be detected simultaneously.

There are several methods for immunostaining using antibodies from the same species, such as directly conjugating the primary antibody with a fluorescent dye before usage, pre-labeling the primary antibody with fluorescent Fab antibody fragments (Brown et al., 2004), or by tyramide signal amplification (Toth and Mezey, 2007). I experimented with these methods and focused on tyramide signal amplification since it worked the best for me, and I have since developed a protocol for it (Figure 5). Tyramide signal amplification works by using horseradish peroxidase to catalyze the oxidation of tyramide into a highly reactive intermediate that rapidly reacts with tyrosine residues from proteins in close proximity to the enzyme, forming a covalent bond with it (Bobrow et al., 1989). By using fluorescently-labeled tyramide molecules and attaching the horseradish peroxidase to the secondary antibody, a fluorescent signal will be deposited at the site of the detected epitope.

Due to the enzymatic signal amplification, a much smaller amount of primary antibody is needed compared to conventional staining. This allows another staining to be done with a standard amount of antibody of the same species after the first staining, since the first staining uses too little primary antibody to be detected by conventional fluorescent secondary antibody staining. Hence, there will not be signal bleed through from the first staining step into the second staining step. Therefore, in our optimized protocol, we first used a 1:5000 dilution of the anti-pSmad2 antibody together with tyramide amplification, and next used a 1:100 dilution of the anti-pSmad5 antibody. Through this protocol, I was able to achieve a double stain of both pSmad2 and pSmad5, which was used in the publication titled “Integration of Nodal and BMP signaling by mutual signaling effector antagonism” (Appx. 5). Using a much smaller amount of primary antibody also has an added benefit of reducing

unspecific background, and was found to be superior to the previously published protocol (van Boxtel et al., 2015) and was therefore used in the publication titled “Scale-invariant patterning by size-dependent inhibition of Nodal signalling” (Appx. 4).

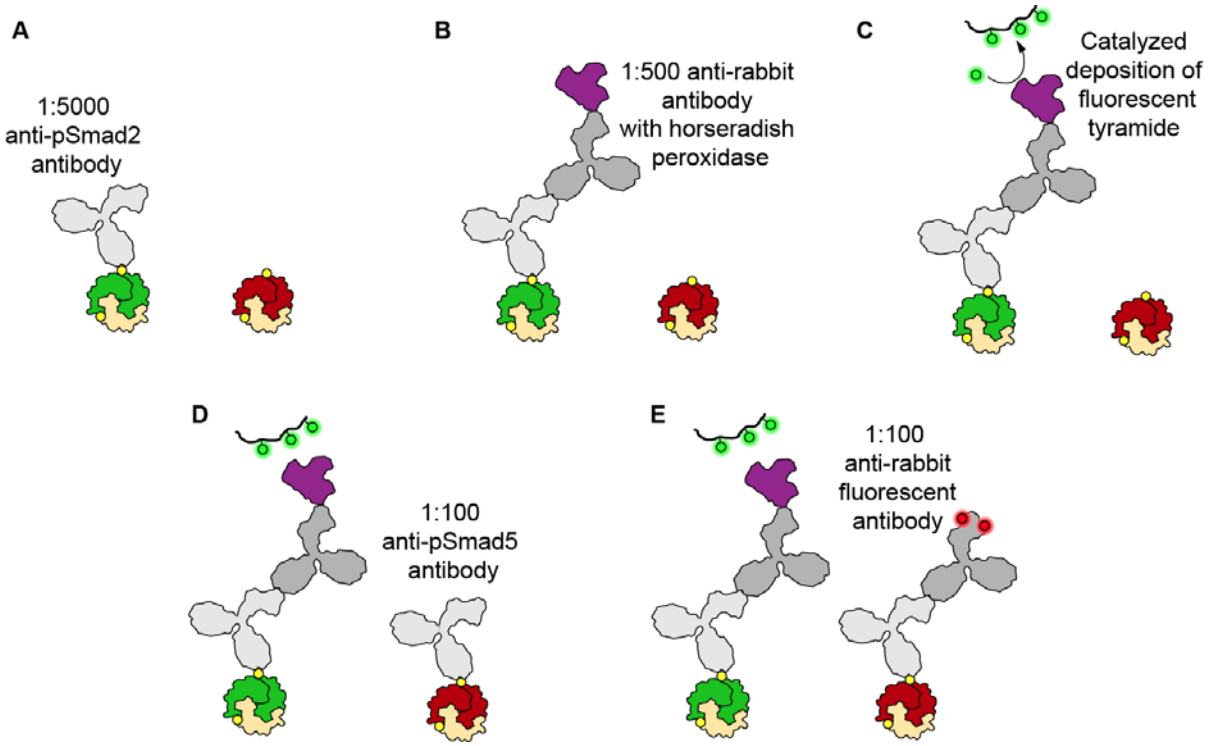

Figure 5: Double pSmad2 and pSmad5 immunostaining protocol. (A) The protocol starts by first staining the embryo with a very low concentration (1:5000) of anti-pSmad2 antibody, **(B)** followed by incubation with a secondary antibody fused to horseradish peroxidase (1:500). **(C)** The horseradish peroxidase then catalyzes the deposition of fluorescently-labelled tyramide to tyrosine residues in neighboring proteins. **(D)** A standard concentration (1:100) of anti-pSmad5 antibody is then used. **(E)** Since the anti-pSmad2 antibody concentration is too low to be detected by conventional fluorescent immunostaining, the subsequent fluorescently-labelled secondary antibody will bind preferentially to the anti-pSmad5 antibody.

Now that a staining protocol has been optimized, a method of visualizing the detected signals is needed. In the case where only a small region at the center of the animal pole needs to be measured, a simple Z-stack followed by a maximum intensity projection is sufficient. However, when the pSmad signal in the entire embryo as a whole needs to be quantified, a maximum intensity projection leads to distortion in lengths at the margin due to the curvature of the embryo. Since the embryo is spherical and the signaling occurs at the surface, cartographical methods of map projections (Figure 6) can be used instead to flatten out the embryo in a projection that maintains length proportions in the direction of quantification (Schmid et al., 2013). The 3D images required for generating the map projection can be made from a Z-stack of multiple 2D images taken throughout the diameter of the embryo. Such

optical sections have been previously made using confocal microscopy, but confocal microscopy suffers from limited penetration in thick samples and a much worse Z- resolution compared to XY-resolution. Selective plane illumination microscopy (SPIM) can overcome these problems (Huisken et al., 2004). SPIM achieves optical sectioning by selectively illuminating the sample with a plane of light from the side, orthogonal to the detection axis. Since only the focal plane is illuminated, no out-of-focus fluorescence is generated and optical sectioning is achieved. However, due to the thickness of the sample, the images get blurred as the focal plane moves away from the microscope objective. This problem is solved by rotating the embryo so that image stacks can be taken from various sides, and then using a software to reconstruct them into a single 3D image (Figure 6A) using bead-based registration (Preibisch et al., 2010)

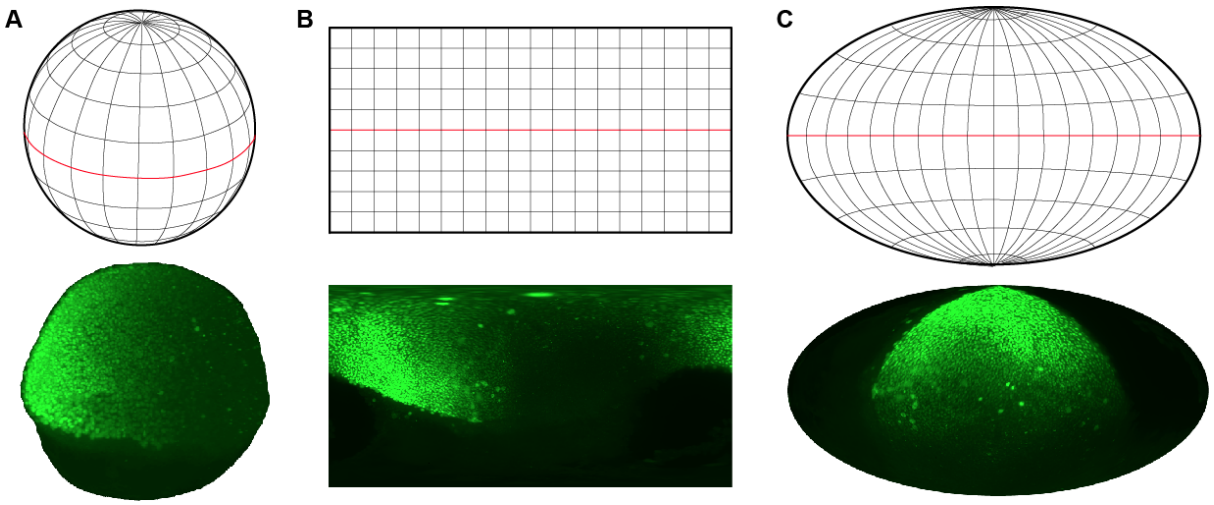

Figure 6: Generation of 2D map projections from 3D embryo reconstructions. (A) 3D reconstruction of embryos stained for pSmad1/5/8 after SPIM imaging. **(B)** Un-oriented 2D map projection in equirectangular projection generated by the Fiji plug-in (Schmid et al., 2013). **(C)** Properly oriented 2D map projection converted to Hammer projection after realigning with the Hugin panorama photo stitcher software.

However, the orientation of a 3D reconstruction can differ from sample to sample due to the calculations the software performs and the orientation of the samples, and this affects the orientation of the 2D map projection that is generated (Figure 6B). This creates a problem as the 2D map projection has to be oriented along the desired embryonic axis to allow quantification. Earlier attempts were made in the lab to realign the orientation of the 3D projection by digitally reslicing it with Imaris, but the process is computationally intensive and takes a long time to complete. I came to realize that a 2D map projection already contains all the needed information of the spherical embryo and that the reorientation can be done with

it directly, making it far less computationally intensive than the reorientation and reslicing of the 3D reconstruction. Therefore, we searched for appropriate software online and found that the Hugin panorama photo stitcher software (http://hugin.sourceforge.net) can be used to reorient the 2D projections (Figure 6C). This method was then applied for the publications titled “Scale-invariant patterning by size-dependent inhibition of Nodal signalling” (Appx. 4) and another titled “Dynamics of BMP signaling and distribution during zebrafish dorsal-ventral patterning” (Appx. 1).

5.3 *in vitro* platform for FRAP experiments

Fluorescence Recovery After Photobleaching (FRAP) assays were developed more than 40 years ago (Liebman and Entine, 1974; Poo and Cone, 1973) and have been used extensively since to measure the diffusion of biomolecules in living tissues. In FRAP assays, fluorescent molecules are bleached in a selected region by exposing it to an intense laser pulse, and the amount of unbleached molecules entering the bleached area afterwards over time is measured by quantitative microscopy (Figure 7A). Mathematical models describing the recovery process are then fitted to the generated recovery curve to determine the diffusion coefficient (Figure 7B). Diffusion measurements can also be done with a complementary approach, called inverse FRAP (iFRAP) (Bläßle et al., 2018). In an iFRAP experiment, fluorescent molecules in a defined area are photoactivated or photoconverted into another emission wavelength (instead of being bleached as in the case of FRAP), and the dissipation of the photoactivated or photoconverted molecule out of the converted area is recorded. The use of photoconversion instead of bleaching has the benefit of using a milder laser pulse, as exposure to intense laser light is damaging to living cells. This measurement instead generates a decay curve which can also be used to determine the diffusivity of the fluorescent molecules with mathematical modelling.

Hence, mathematical models are crucial requirements to extract the diffusion coefficient from raw FRAP data. Early models make several simplifications (Axelrod et al., 1976), such as reducing the experimental system to a one-dimensional or two-dimensional model, assuming that the pool of fluorescent molecules is infinitely large, or ignoring the complex geometries of biological samples which affect the movement of macromolecules. Thus, many new models implemented in various software have been designed to take these factors into consideration and produce more accurate results (Bläßle et al., 2018; Blumenthal et al., 2015; Rapsomaniki et al., 2012; Schaff et al., 2009). Therefore, in order to test and benchmark new

as well as existing models, I have created an *in vitro* system (Figure 7C). An *in vitro* system has an advantage in performing such benchmarking since it excludes confounding factors such as cell movement, or the production or degradation of fluorescent proteins.

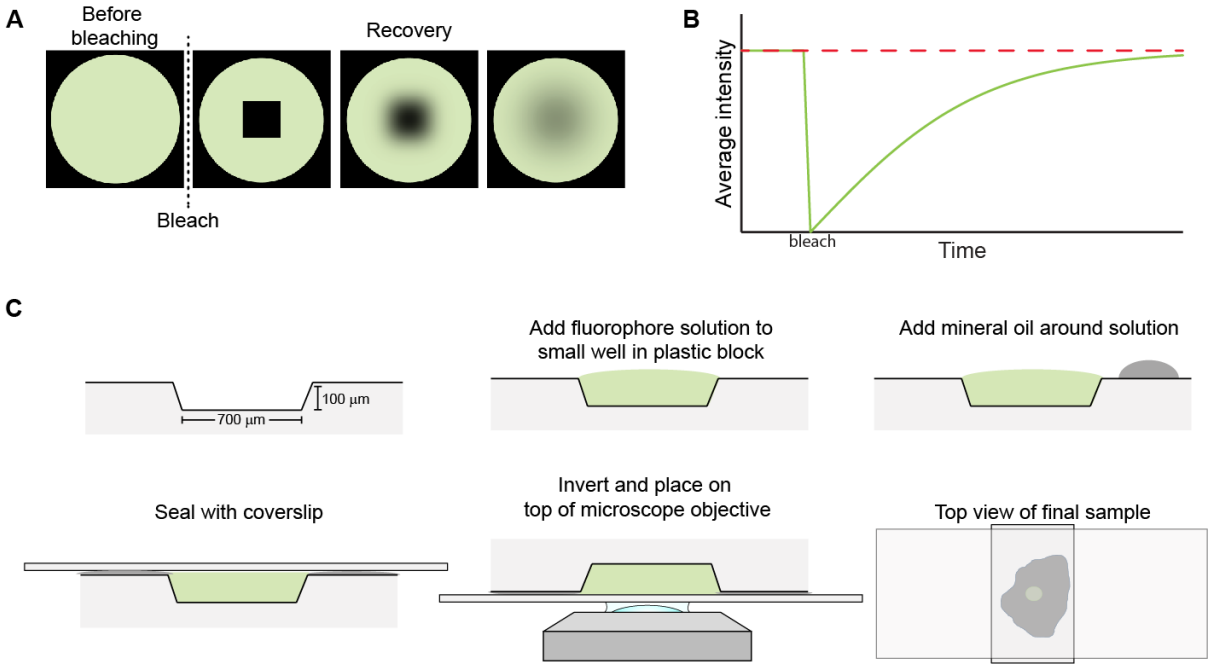

Figure 7: *in vitro* FRAP experiment system. (A) During FRAP, a region of the sample is bleached by an intense laser pulse. The fluorescent molecules in the unbleached area then diffuse into the bleached area, and the rate of fluorescent recovery is measured. **(B)** Measured intensity of the bleached area before and after bleaching. The measured recovery curve can then be fitted with a mathematical model to derive the diffusion coefficient of the fluorescent molecule. **(C)** The *in vitro* FRAP experiment is carried out in a plastic block with a small well. The fluorophore solution is first pipetted into the well, and mineral oil is then pipetted around the well, so that it completely surrounds the well. A rectangular coverslip is then placed over the well. The sample is then inverted for imaging in an inverted confocal microscope.

The *in vitro* system consists of a ~10 mm thick transparent and colorless plastic block with a hole ~700 µm in diameter and ~100 µm in depth made with a dental drill, with the size chosen so that it has similar dimensions as a zebrafish sphere-stage embryo. A solution containing fluorescent molecules is then pipetted into the well, and a ring of mineral oil is pipetted around the well. The mineral oil is needed to allow the plastic block to adhere via capillary action to the glass coverslip which will be placed over the well. The plastic block is then carefully flipped over so that the sample can be imaged on a confocal inverted microscope. This creates a cylinder of fluorescent solution with a known volume in which FRAP experiments can be done. Since the diffusion coefficients of macromolecules in solution can be calculated via the Einstein-Stokes equation if the molecular weight is known, we can carry out benchmarking FRAP experiments with fluorescently-labelled dextrans of

known molecular weight in the *in vitro* system. We can thus compare the diffusion coefficient calculated from the recovery curve using the different recovery models with the diffusion coefficient calculated from the Einstein-Stokes equation. This allows us to detect if there are any irregularities in the model or the microscope setup if we see a significant deviation between the predicted and the measured diffusion coefficient.

In biological samples, the movements of macromolecules are often hindered by presence of physical obstacles such as cells or extracellular matrix. The macromolecules have to go around these obstacles, effectively slowing them down and reducing their effective diffusion coefficient. This effect is known as tortuosity. The *in vitro* system can also be modified to account for tortuosity by mixing polyacrylamide microbeads into the solution before adding into it the well, which mimics the tortuosity caused by cells (Appx. 2, Figure 4I).

In the paper titled "Quantitative diffusion measurements using the open source software PyFRAP" (Appx. 2), we used the *in vitro* system as a means of testing the functionality and analytic capabilities of the FRAP analysis software 'PyFRAP'. We carried out FRAP experiments *in vitro* of fluorescein-dextrans with sizes varying over two orders of magnitude as well as purified GFP, and performed iFRAP experiments with purified Dendra2. We found that PyFRAP outputs diffusion coefficients which match both theoretical predictions and previous literature values. We also carried out *in vitro* experiments in the presence of polyacrylamide beads and found a reduction in the effective diffusion rate by 18% for purified GFP, and a 39% reduction for 70 kDa fluorescein-dextran. The systematic protocol for the use of the *in vitro* system, as well as a protocol for conducting FRAP experiments in zebrafish embryos and how to analyze them with PyFRAP was then detailed in the book chapter "FRAP Analysis of Extracellular Diffusion in Zebrafish Embryos" (Appx. 3).

5.4 Biophysical characterization of the BMP/Chordin system

With the methods I developed, we first directed our attention towards understanding the interactions between BMP and Chordin. There are currently a number of competing models describing their interactions (Appx. 1, Figure 1). The current popular model is the 'Shuttling model' mentioned above (Ben-Zvi et al., 2008), which posits that the more diffusive Chordin enhances the diffusivity of BMP upon binding, allowing it to shuttle BMP from the dorsal to the ventral side (Chordin is produced on the dorsal side). However, several other possible models have been posited as well. The first model is the 'graded source-sink with mobile

BMP' where BMP is produced in a gradient, which is highest on the ventral side (the 'source'). BMP then diffuses across the embryo, forming a gradient. BMP signaling is excluded from the dorsal side by binding to a gradient of Chordin produced from the 'sink', a localized region on the dorsal side. The interaction between these two gradients, a BMP 'source' and a Chordin 'sink' leads a ventral to dorsal gradient of BMP activity (detected as the presence of pSmad5). The 'graded source-sink with immobile BMP' is similar; however, it is based on evidence that suggests that BMP does not diffuse (Ramel and Hill, 2013). Another model, the 'long-range accumulation and feedback' model, assumes diffusive BMP and Chordin, but their interaction is controlled by differences the stability of BMP and Chordin (Inomata et al., 2013). In this model, BMP signaling induces Sizzled which blocks the proteolysis of Chordin by Tolloid, causing Chordin to expand ventrally, suppressing BMP signaling. This triggers a feedback response since the reduction of BMP signaling also leads to the reduction of Sizzled production, which would lead to enhanced degradation of Chordin and consequently an increase in BMP signaling activity. The 'self-regulating reaction-diffusion system' model instead assumes that both BMP and Chordin have a low diffusion coefficient and similar protein stability, while Sizzled and ADMP (a secreted protein produced in the dorsal side with BMP signaling activity (Lele et al., 2001) that can inhibit Chordin production) having a high diffusion coefficient. BMP then forms a reaction-diffusion system with Sizzled, and Chordin with ADMP, whereby the highly diffusive Sizzled and ADMP regulate the ranges of BMP and Chordin. This creates a robust self-regulating system during embryogenesis (François et al., 2009). Therefore, we can see that these models make different predictions about the biophysical properties of BMP and Chordin, as well as accessory proteins such as Sizzled and ADMP, and the pSmad5 distribution with and without Chordin. Hence, characterizing the biophysical properties of BMP, Chordin, Sizzled and ADMP, together with the pSmad5 distribution in wild type embryos and *chordin* mutants is crucial to identify the correct model that explains their interaction.

To this end, we generated functional fluorescent and photoconvertible fusion constructs of Bmp2b, Chordin, Sizzled and ADMP for FRAP and FDAP experiments. We transplanted cells expressing these fluorescent versions into host embryos and found that Bmp2b and Chordin both generated a gradient when produced from a localized source (Appx. 1, Figure 3). I also expressed them in embryos and used FRAP to measure the diffusion coefficient of Bmp2b and Chordin, which was found to be 2–3 $\mu m^2/s$ and 6–7 $\mu m^2/s$ respectively (Appx. 1, Figure 4E). Strikingly, there was no significant difference in the diffusion coefficient of

Bmp2b when coexpressed with Chordin. Sizzled was found to have a diffusion coefficient 9.7 ± 3.2 $\mu m^2/s$, but we were unable to measure the diffusion coefficient of ADMP as we were unsuccessful in creating fluorescent ADMP fusions that has similar activity as its untagged version. We also found that Bmp2b has a half-life of 130 min, while Chordin has a half-life of 120 min (Appx. 1, Figure 4A+B). We then measured the pSmad5 distribution in wild type and *chordin* mutants after 2D map projection (Appx. 1, Figure 1+2). In wildtype embryos, BMP signaling starts from a low-level near-uniform distribution to a gradient with peak intensity levels on the ventral side. In *chordin* mutants, the ventral side had slightly higher pSmad5 signaling, but the spatial extent is greatly expanded to the dorsal side.

We can draw four main conclusions from our biophysical data. First, BMP2b and Chordin are found to be able to diffuse in the extracellular space. Second, fluorescently tagged BMP2b, Chordin and Sizzled have diffusivities in the same order of magnitude. Third, Chordin does not significantly change BMP2b diffusion when expressed together. With these results, we can start to identify the model most appropriate in explaining the interactions between BMP and Chordin.

5.5 BMP interacts with Chordin via a source-sink mechanism

With the biophysical and signaling data at hand, we can look for the model which best fits the data. The prominent ‘shuttling model’ proposes that Chordin reversibly binds to BMP, which enhances its diffusivity. This increase in diffusivity causes BMP to be shuttled from the dorsal to the ventral side (Ben-Zvi et al., 2008). However, we do not detect any increase in the diffusion coefficient of Bmp2b when it is co-expressed with Chordin (Appx. 1, Figure 4E), undermining one of the key predictions of the ‘Shuttling model’. Moreover, when we transplanted a fluorescent BMP source juxtaposed with a Chordin source, we found that the BMP gradient was not altered by the presence of Chordin (Appx. 1, Figure 5). Hence, we conclude that the shuttling model is not applicable for zebrafish. The ‘self-regulating reaction-diffusion system’ model relies on Sizzled having a much higher diffusion coefficient than BMP or Chordin (François et al., 2009), but our FRAP results show that the diffusion coefficient of Sizzled is too slow to fit this model (Appx. 1, Figure 4E). As for the ‘long-range accumulation and feedback’ model, our FDAP measurements do not detect significant differences between BMP and Chordin protein stability (Appx. 1, Figure 4A+B), contradicting the core assumptions of that model (Inomata et al., 2013). In our transplantation experiments using a BMP source, we found that BMP is secreted and capable of generating a

gradient around its source cell (Appx. 1, Figure 3). This refutes the 'graded source-sink with immobile BMP' model, which posits an immobile BMP. Thus, the 'graded source-sink with mobile BMP', which describes a system in which diffusive BMP (which is secreted from a ventrally biased 'source') is inhibited by an similarly diffusive Chordin (secreted from a dorsal 'sink') to generate the BMP signaling gradient, is the sole remaining model that fits the biophysical data from our experiments (Figure 8).

Another additional observation that *chordin* mutants can be rescued by homogeneous expression of Chordin throughout the whole embryo by mRNA injection (Schulte-Merker et al., 1997), and a similar rescue of BMP mutant embryos by homogeneous expression of BMP (Appx. 1, Figure 3C) also supports the 'graded source-sink with mobile BMP' model. Since Chordin acts as an inhibitor of BMP signaling instead of a shuttle, a homogenous production of Chordin at a specific concentration can ensure that the resulting pSmad5 gradient is correctly formed by globally suppressing BMP signaling as long as BMP is present in a graded source. The inverse is also true for the rescue of BMP mutants, although in this case, it is the graded Chordin source which sculpts the resulting pSmad5 gradient by selectively inhibiting it on the dorsal side. However, we observed that rescue requires specific concentrations of BMP or Chordin. Hence, the 'source-sink' system can be seen as a way to make the system more robust to developmental noise by imposing a self-regulatory system that balances between BMP and Chordin.

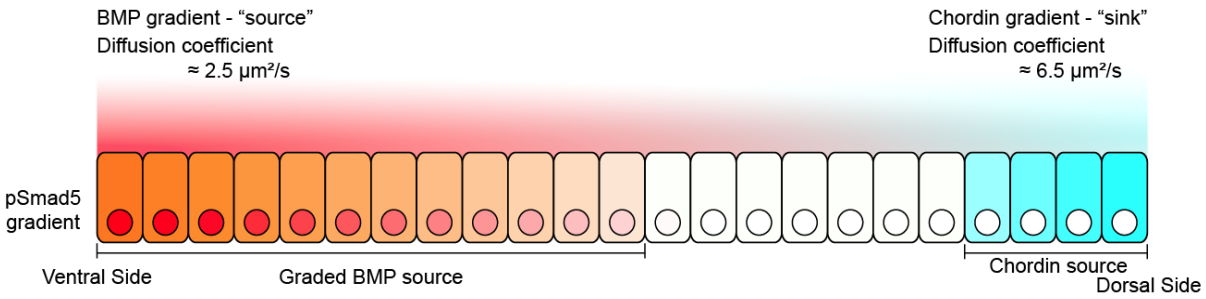

Figure 8: Graded source-sink model of BMP and Chordin interaction. In this model, BMP and Chordin are secreted and diffuse from graded sources at the ventral and dorsal side respectively. Chordin acts as a 'sink' which suppresses BMP activity at the dorsal side, causing pSmad5 activity to be restricted to the ventral side.

However, this model is still incomplete. For instance, it has been reported that there is BMP expression at the dorsal side which regulates the expression of Chordin (Xue et al., 2014). The authors report pSmad5 activity in the dorsal side, which we do not observe. This model also does not include other molecules known to regulate BMP activity, such as Sizzled and

Tolloid (Blader et al., 1997; Muraoka et al., 2006). Moreover, it does not account for the presence of ADMP, which is known to be critical in dorso-ventral patterning in *Xenopus* frogs (François et al., 2009) but its role in zebrafish is poorly understood with only a few publications on it so far (Dickmeis et al., 2001; Lele et al., 2001; Willot et al., 2002; Yan et al., 2019). Another aspect that is still lacking in the model is that it is cannot explain the phenomenon of scaling, whereby the embryo can develop normally even if its size is experimentally reduced. The other models, such as 'shuttling model', the 'self-regulating reaction-diffusion model' and the 'long range accumulation and feedback model' became attractive because they account for scaling (Ben-Zvi et al., 2008; François et al., 2009; Inomata et al., 2013). Although theoretical possibilities for scaling in such a system exists (Howard and ten Wolde, 2005; McHale et al., 2006), more work needs to be done to see if they fit experimental observations.

5.6 Nodal and BMP signal at different ranges due to differences in their signaling activity

With the biophysical properties of BMP and Nodal measured (Müller et al., 2012; Pomreinke et al., 2017), and models for how they interact with their inhibitor established (Müller et al., 2012; Pomreinke et al., 2017; van Boxtel et al., 2015), I decided to direct my focus to how they signal and interact with each other. Earlier results have shown that ectopic expression of different ratios of Nodal and BMP can generate various ectopic structures (Fauny et al., 2009), and juxtaposed sources of Nodal and BMP can induce the formation of a secondary axis (Xu et al., 2014). Thus, it is apparent that Nodal and BMP are sufficient to trigger the formation of an embryonic axis. We see this phenomenon of secondary axis formation by ectopic sources as an experimentally tractable model system to study Nodal and BMP signaling because it allows us to use ectopic gradients that mimic something that is physiologically relevant, namely axis induction. This frees us from relying solely on endogenous gradients which are challenging to study due to the difficulty in making fluorescent knock-ins, or controlling the timing and intensity of their gradients.

With my functional fluorescent Nodal and BMP constructs, I can create gradients that I can measure. With my protocol that allows us to detect both pSmad2 and pSmad5, I can directly measure the primary signaling output of Nodal and BMP, respectively. Hence, this model system allows us to directly study the signaling input-output relationships of Nodal and BMP

signaling and understand how they are integrated to form an embryo. Using my transplantation device, I transplanted fluorescent sources of Nodal and BMP and successfully used them to generate secondary axes in the host embryos. I was able to measure both the fluorescent gradient as well as the resulting pSmad signals, and I found that the Nodal source generates a localized, short range pSmad2 gradient, which is overlaid by an extensive pSmad5 gradient generated by the BMP source (Appx. 5, Figure 1B+C). This starkly contrasts with the protein gradients of Nodal and BMP emanating from respective sources, which we observe to be of similar range (Appx. 5, Figure 1B+C).

In order to relate the ligand gradients to the signaling ranges, I developed a method to quantify the absolute concentrations of the ectopic Nodal and BMP gradients based on their fluorescence intensities (Appx. 5, Supp. Figure 4). I purified recombinant sfGFP and mVenus proteins and generated calibration curves on the microscope, which allowed me convert the detected fluorescence intensities to their molar concentrations. I then used these calibration curves to determine the molar concentrations of the gradients of fluorescently-tagged Nodal and BMP expressed from local sources in zebrafish embryos. This allowed me to compare the ligand concentrations of the Nodal and BMP gradients. In doing so, I discovered that the difference in their pSmad ranges, with Nodal having a short pSmad2 range and BMP having a long pSmad5 range, occurs even though their gradients are of similar range, shape and amplitude.

I therefore hypothesized that the different signaling ranges from similar input gradients might be due to differences in their signaling activation kinetics. According to the law of mass action and Hill kinetics, signals with higher sensitivity can induce activation faster – leading to a longer signaling range, whereas signals with low sensitivity would require extended exposure until activation is induced in a threshold-type manner – leading to a shorter signaling range (Michaelis et al., 2011). We developed a mathematical model based on Hill kinetics and showed that the value of the pSmad activation term (which combines the activation kinetics of the morphogen for their receptors as well as the pSmad activation rate of said receptors) can control the signaling range of the morphogen (Appx. 5, Figure 3B).

To test this idea, I took advantage of the recent discovery that a single source of mouse BMP4 can generate a secondary zebrafish axis (de Olivera-Melo et al., 2018), which suggested the possibility that mouse BMP4 might carry both BMP and Nodal signaling

activities. I transplanted clones expressing mouse BMP4 into zebrafish embryos and found that they do indeed induce both pSmad2 and pSmad5 (Appx. 5, Figure 3C). Strikingly, mouse BMP4 clones induce pSmad2 at a short range, while inducing pSmad5 at a long range, supporting my model that the exact same gradient can induce effector activation at different ranges solely due to differences in signaling activity.

If this is indeed the case for Nodal and BMP, then BMP with its high signaling activity should be limited by its diffusion coefficient, whereas Nodal, with lower signaling activity, should be limited by its signaling activity rather than its diffusivity. To test this, I perturbed the protein distributions of Nodal and BMP using morphotraps, transmembrane proteins with anti-GFP nanobodies on the extracellular side that can drastically reduce the diffusivity of extracellular proteins tagged with GFP derivatives (Almuedo-Castillo et al., 2018; Harmansa et al., 2017; Mörsdorf and Müller, 2019), and found that BMP signaling range is drastically reduced, while the signaling range of Nodal is mildly reduced (Appx. 5, Figure 3G). Therefore, differences in signaling kinetics can be considered as an additional knob to tune the signaling ranges of morphogens (Figure 9), in addition to differences in diffusivity and clearance (Rogers and Müller, 2019), and may play a role in restricting Nodal signaling to the margin. Hence, future studies on morphogens have to take their signaling activity into account as well.

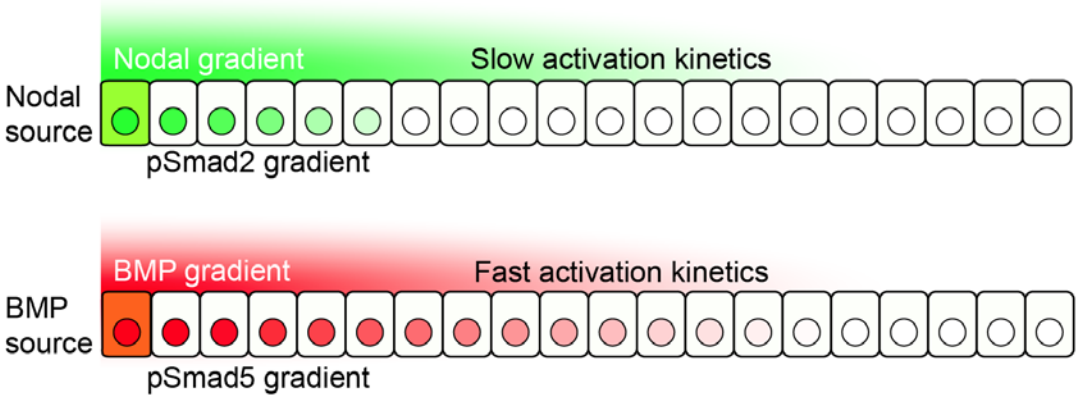

Figure 9: Differential signaling activation kinetics allows Nodal and BMP to have different signaling ranges. The slow activation kinetics of Nodal cause it to generate a shorter pSmad2 gradient, while the fast activation kinetics of BMP cause it to make a broad pSmad5 gradient, even when they have protein gradients of similar ranges.

Interestingly, a similar difference in signaling dynamics was also found between exogenously added ACTIVIN and BMP4 in micropatterned colonies of mouse embryonic stem cells. ACTIVIN initially activates SMAD2 rapidly but also decreases quickly and is maintained at

a low level, while BMP4 activates SMAD1 slowly but increases over time and is maintained at a high level (Yoney et al., 2018). Like in the case for Nodal and BMP in zebrafish, this leads to ACTIVIN having a longer range compared to BMP4 when added to mouse embryoid bodies. Hence, it may be a general principle for ligands which rapidly activate their effector to have a longer range while ligands which slowly activate their effector to have a shorter range.

Another interesting observation we made is that the progression and shape of the Nodal and BMP gradients (Appx. 5, Figure 2G+H) differ from the pSmad2 and pSmad5 gradients (Appx. 5, Figure 2C+F), respectively. For Nodal signaling, I notice that pSmad2 peaks just as the Nodal protein gradient declines. As for BMP, pSmad5 signal starts off high but starts declining after 1 hour even though the BMP gradient stays constant. The decrease in pSmad5 intensity was also observed in *chordin* morphants, arguing against Chordin being responsible for this decline (Blader et al., 1997; Fisher and Halpern, 1999; Schulte-Merker et al., 1997). Hence, other Chordin-independent BMP feedback inhibitors such as Bambia or Smad7 might be responsible for this downregulation of BMP signaling over time (Pogoda and Meyer, 2002; Tsang et al., 2000). However, it is also possible that this could be due to internalization and degradation of BMP receptors or the action of an unknown phosphatase induced by BMP signaling (Alborzinia et al., 2013; Bruce and Sapkota, 2012). Such deviation of the protein gradient from the activity gradient was also observed for the BMP homolog Dpp in the *Drosophila* wing disc (Teleman and Cohen, 2000). Hence, these results caution that a signaling gradient at a particular moment need not directly correspond to the current protein gradient. Future experiments involving fluorescent morphogen knock-ins will have to take into account the possible discrepancy between ligand distribution and signaling response.

5.7 Nodal and BMP are capable of signaling directly

With this model system established, I directed my attention to resolving the current controversy on whether Nodal and BMP signal directly or through a relay mechanism (Chen and Schier, 2001; Müller et al., 2012; Pomreinke et al., 2017; Ramel and Hill, 2013; Rogers and Müller, 2019; van Boxtel et al., 2015; Zinski et al., 2017). Earlier results utilized mesodermal gene induction as a readout of Nodal signaling in order to show that Nodal diffuses and can signal directly at a distance (Chen and Schier, 2001). This result has recently been called into question by findings that show that the mesoderm-inducing activity of Nodal

is in part due to a relay mechanism involving FGF (Mathieu et al., 2004) and the observation that Nodal signaling is restricted to areas of Nodal mRNA expression in embryos, which is indicative of it being spread through a relay mechanism (van Boxtel et al., 2015). Similarly, BMP signaling is observed to be restricted to where BMP mRNA is expressed (van Boxtel et al., 2015), and studies analyzing BMP signaling from an ectopic source have not been done. Since I have the ability to image the immediate signaling output of Nodal and BMP, I can settle this issue by looking at the pSmad gradients directly.

I used my transplantation device to generate localized sources of fluorescently-tagged Nodal and BMP in *MZsqt;cyc* (lacks functional Nodal) and *MZswr* (lacks functional BMP) mutants respectively, which allowed me to test the possibility of a signaling relay. I discovered that both Nodal and BMP can directly activate their respective Smads at a distance, supporting the idea that they can function as morphogens (Appx. 5, Figure 2B+E). This contradicts the other finding that they signal through a relay and that their Smad signaling activity is located only in the Nodal or BMP expression domain respectively (Ramel and Hill, 2013; van Boxtel et al., 2015). However, I believe that this contradiction can be resolved as follows. Nodal signaling triggers its own expression (Mathieu et al., 2004) in wildtype embryos, but this genetic circuit are balanced by the short signaling range of Nodal in a way that cause Nodal signaling to appear restricted to areas of Nodal expression as if Nodal does not diffuse; if Nodal signaling had higher signaling affinity instead, we would see Nodal signaling appearing outside areas of Nodal expression in wildtype embryos. For BMP, my rescue of *MZswr* mutants with a BMP transplant (Appx. 5, Figure 2A) shows that an isotropic BMP protein gradient can form a normal embryo. This means that the dorsally secreted BMP inhibitors are sufficient to shape the pSmad5 gradient without need for a graded expression of BMP. Thus, the graded expression of BMP is perhaps a means of ensuring developmental robustness and is not strictly essential. A similar effect is seen where a graded expression of Lefty can be compensated by using a specific concentration of a Nodal inhibiting drug (Rogers et al., 2017), and where *chordin* mutants can be rescued with a specific amount of uniformly expressed *chordin* mRNA (Schulte-Merker et al., 1997). This also supports our earlier results on the ‘source-sink model’ of BMP signaling, which shows that the shape of BMP expression profile contributes to the shape of the pSmad5 gradient, but its shape ultimately depends on its interaction with the Chordin ‘sink’. Therefore, despite Nodal and BMP appearing to be non-diffusive as their signaling is found where they are produced, when they are tested in an

isolated manner via an ectopic source in mutants, we see that are intrinsically able to diffuse and signal directly at a distance.

5.8 Nodal and BMP selectively antagonize each other via Smads

The use of this model system also revealed that the double transplants generate a region of highly localized pSmad2 activity overlaid on a broad distribution of pSmad5 activity. To test whether the observed region of mixed pSmad2 and pSmad5 activity is responsible for secondary axis induction, I generated embryos in which I activated specific ratios of Smads in a localized region independently of Nodal and BMP using constitutively active Smads. The constitutively active Smad2 (Smad2-CA) and Smad5 (Smad5-CA) were made by exchanging their three C-terminal serines with aspartates, and they were expressed in a localized region in the embryo to observe their effects (Appx. 5, Figure 4A). In doing so, I found that these constitutively active Smads do indeed generate different ectopic structures when expressed in different ratios (Appx. 5, Figure 4B–F). Injecting *smad2-CA* mRNA alone generated an ectopic trunk structure containing axial tissues, while injecting *smad2-CA* mRNA mixed with increasing amounts of *smad5-CA* mRNA induces more ventral structures. Using *smad2-CA* mRNA and *smad5-CA* mRNA in a 1:1 ratio led to structures with ectopic hindbrains and in some cases led to a secondary axis, while a four-fold excess of *smad5-CA* mRNA over *smad2-CA* mRNA generates ectopic tails. These ectopic structures can be generated even when the Nodal and BMP receptors are inhibited, indicating that they do not need any further auto-inductive signal relay through Nodal or BMP.

The fact that varying amounts of ectopically-expressed, constitutively active Smads can generate ectopic structures is an intriguing discovery that builds on previous work where ectopic expression of different amounts of Nodal and BMP generates different ectopic structures (Fauny et al., 2009). This shows that varying ratios of Smads are the main molecular factors that relay the inductive capabilities of Nodal and BMP. The inductive properties of various ratios of constitutively active Smads also highlight an intriguing possibility; just like the Yamanaka factors can be used to convert differentiated cells into pluripotent cells (Takahashi and Yamanaka, 2006), it could also be possible to use specific ratios of these two Smads to induce morphogenesis of pluripotent cells and specify them into the desired embryonic structures. This directed differentiation of stem cells could play a key role in regenerative medicine.

In the zebrafish embryo, Nodal and BMP (and consequently pSmad2 and pSmad5) are generated in an overlapping and orthogonal manner (Appx. 5, Figure 5A). Hence, there are regions where pSmad2 is present, regions where pSmad5 is present, regions where both pSmad2 and pSmad5 is present, regions where neither is present, and regions where either pSmad2 or pSmad5 is present but without the other. Therefore, there has to be a mechanism for cells to respond differently to different ratios of pSmad2 and pSmad5 as we observed that different embryonic structures can be generated by the differing ratios. We know that certain Nodal target genes are only found in regions without BMP signaling, and likewise for BMP target genes. For instance, *gsc* is induced by Nodal signaling (Bennett et al., 2007; Gritsman et al., 1999) but only expressed at the dorsal margin (despite pSmad2 activity being found in the entire margin), suggesting that it is induced by high pSmad2 and low pSmad5 levels; *foxi1* is a BMP target gene and an epidermal marker that is expressed on the ventral side but is excluded from the ventral margin (Hans et al., 2007) (despite pSmad5 signaling also being present in the ventral margin), suggesting that is induced by high pSmad5 and low pSmad2 levels. We also know that *eve1* is expressed in the ventral margin (where both pSmad2 and pSmad5 are active) and is a marker for ventral mesoderm (Joly et al., 1993), suggesting that it is induced by both high pSmad2 and high pSmad5 levels. Knowing how these genes are selectively induced by different ratios of Nodal and BMP signaling will bring us closer to understanding how different embryonic structures are induced by the differing ratios of Nodal and BMP signaling. Therefore, in order to find out how ratio specific target gene activation occurs, I injected embryos with different ratios of *smad2-CA* and *smad5-CA* mRNA and assessed their expression with fluorescent *in-situ* hybridization.

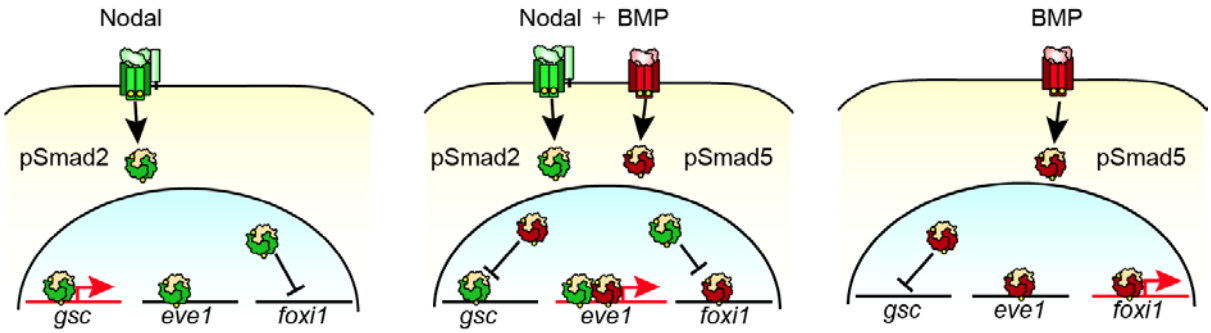

Figure 10: Selective mutual antagonism of pSmad2 and pSmad5 provides a mechanism that allows cells to express different set of genes in response to different ratios of Nodal and BMP signaling. The selective antagonism of Smad2 to the expression of *foxi1* and Smad5 to *gsc* expression allows cells with both high Smad2 and Smad5 to express *eve1* without expressing *foxi1* or *gsc*. The arrows showing activation or inhibition are an abstraction, and the underlying mechanisms may be direct or indirect.

Interestingly, I found that Smad2-CA and Smad5-CA selectively antagonize each other for the induction of *gsc* and *foxi1*, whereas *eve1* showed a biphasic sensitivity to these signaling effectors (Figure 10). Smad2-dependent *gsc* expression was suppressed when high levels of Smad5-CA co-expressed with high levels of Smad2-CA (Appx. 5, Figure 5B), and Smad5-dependent *foxi1* expression was inhibited by high Smad2-CA levels when co-expressed with high Smad5-CA (Appx. 5, Figure 5C). Strikingly, *eve1* was induced synergistically when both Smad2-CA and Smad5-CA are present, and is highest at a moderate amount of Smad2-CA expression (Appx. 5, Figure 5D). In contrast, high amounts of Smad2-CA led to reduced eve1 expression, consistent with the absence of dorsal *eve1* expression (Joly et al., 1993) where Nodal signaling is the strongest and active over a longer period of time (Dubrulle et al., 2015; van Boxtel et al., 2018). These results suggest that Smad2 and Smad5 can selectively antagonize each other for certain genes, which acting synergistically for others, providing a molecular mechanism that allow cells to respond specifically to different ratios of Nodal and BMP signaling.

Similar cases of mutual antagonism also exist in other morphogen pairs, such as the Bicoid and Caudal system (Briscoe and Small, 2015). However, their mutual antagonism is not selective, since Bicoid represses Caudal translation via direct binding to *caudal* mRNA (Niessing et al., 2002). I believe that this selective antagonism is needed because Nodal and BMP form overlapping orthogonal gradients (Rogers and Müller, 2019) instead of antiparallel gradients like that of Bicoid and Caudal. The overlapping nature of the Nodal and BMP gradients will therefore lead to an area having both high pSmad2 and pSmad5 activity, as well as areas with either high pSmad2 or high pSmad5 alone. However, cells in areas with high pSmad2 alone, or high pSmad5 alone do not have the same cell fates as in areas with both high pSmad2 and high pSmad5. Therefore, this mechanism of selective antagonism not only allows the cells to sense the ratio of Nodal and BMP, but can also work when these gradients overlap. This mechanism, due to its straightforward implementation, may also be a general mechanism in play in the case of other overlapping gradients.

6. Conclusion and Outlook

In this dissertation, I sought to further our understanding of morphogens and their role in embryonic development by studying the behavior of Nodal and BMP in zebrafish. Currently, the means by which morphogens spread (by diffusion or other means) and signal (directly or by relay) is still controversial. To solve this, I developed several tools and protocols: a transplantation device, an *in vitro* FRAP assay, a double pSmad immunostaining protocol, and a streamlined pipeline for cartographic projections of Smad immunostains in zebrafish embryos. I then applied them to the study of Nodal and BMP, and provided evidence that both Nodal and BMP can diffuse to form a gradient, and that they both can signal directly at a distance. I also measured the diffusion coefficients of BMP and its inhibitor, Chordin, and with the help of mathematical modelling by the other contributing author Patrick Müller, showed that a source-sink mechanism best explains how Chordin interacts with BMP to generate the pSmad5 gradient. I additionally showed that Nodal has slower activation kinetics than BMP. The slow activation kinetics may help explain why Nodal activity is restricted in a short range around the margin, while BMP activity spreads out halfway across the embryo. I further show that the direct Nodal and BMP effectors, pSmad2 and pSmad5, can induce various ectopic structures when ectopically expressed, and that pSmad2 and pSmad5 selectively antagonize each other for certain genes but not for others. This provides an elegant explanation for how overlapping Nodal and BMP gradients can generate different cell fates and brings us closer to understanding how combined Nodal and BMP signaling interact with each other to generate an embryonic axis.

These results provide strong evidence that Nodal and BMP can function as morphogens, with diffusion playing the main role in the formation of their signaling gradients, and the activation kinetics of their effectors playing an added role in regulating signaling range. However, I am certain that this will not be the last word as more information may be uncovered in the future. For the next few steps ahead, I believe that the generation of transgenic knock-in lines is one of the key experiments to be carried out. With endogenously expressed fluorescent Nodal and BMP, we will be able to use fluorescence microscopy to directly quantify the protein gradients as they form, as well as use the morphotrap to perturb these endogenous gradients. This would allow us to test whether that what we measure for the ectopic gradients is also true for the endogenous case. Currently, there has been an expansion of new transgenic knock-ins due to the discovery of the Clustered, Regularly Interspaced,

Short Palindromic Repeat (CRISPR)/CRISPR-associated 9 (Cas9) system which simplifies the process compared to earlier approaches with transcription activator-like effector nucleases (TALEN) and zinc finger nucleases (Doyon et al., 2008; Hruscha et al., 2013; Zu et al., 2013). However, the method is still somewhat inefficient for zebrafish, but an effective protocol may eventually be developed in the future.

Another important task for future research is to unravel the mechanism that allows pSmad2 and pSmad5 to selectively inhibit each other for certain cell fates and to utilize the ability of different ratios of Smad2-CA and Smad5-CA to generate different embryonic structures *in vitro*. Currently, it is still unclear if the interaction between pSmad2 and pSmad5 is direct. Hence, experiments such as chromatin-immunoprecipitation-sequencing are required to identify the transcription factors behind this selective inhibition. As for the inductive properties of Smad2-CA and Smad5-CA, it would be interesting to test them out on embryos or embryonic stem cells of different species to test if they work in other contexts as well. Success in this endeavor would surely enhance our ability to generate the desired tissue types on demand and may have positive implications for regenerative medicine. With all of these possibilities, I am certain that there will be plenty more excitement to come in the field of developmental biology.

7. References

Alborzinia, H., Schmidt-Glenewinkel, H., Ilkavets, I., Breitkopf-Heinlein, K., Cheng, X., Hortschansky, P., Dooley, S. and Wolfl, S. (2013). Quantitative kinetics analysis of BMP2 uptake into cells and its modulation by BMP antagonists. *Journal of cell science* **126**, 117-127.

Almuedo-Castillo, M., Bläßle, A., Mörsdorf, D., Marcon, L., Soh, G. H., Rogers, K. W., Schier, A. F. and Müller, P. (2018). Scale-invariant patterning by size-dependent inhibition of Nodal signalling. *Nature cell biology* **20**, 1032-1042.

Axelrod, D., Koppel, D. E., Schlessinger, J., Elson, E. and Webb, W. W. (1976). Mobility measurement by analysis of fluorescence photobleaching recovery kinetics. *Biophysical journal* **16**, 1055-1069.

Ben-Zvi, D., Shilo, B. Z., Fainsod, A. and Barkai, N. (2008). Scaling of the BMP activation gradient in Xenopus embryos. *Nature* **453**, 1205-1211.

Bennett, J. T., Joubin, K., Cheng, S., Aanstad, P., Herwig, R., Clark, M., Lehrach, H. and Schier, A. F. (2007). Nodal signaling activates differentiation genes during zebrafish gastrulation. *Developmental biology* **304**, 525-540.

Bisgrove, B. W., Su, Y. C. and Yost, H. J. (2017). Maternal Gdf3 is an obligatory cofactor in Nodal signaling for embryonic axis formation in zebrafish. *eLife* **6**, e28534.

Blader, P., Rastegar, S., Fischer, N. and Strähle, U. (1997). Cleavage of the BMP-4 antagonist chordin by zebrafish tolloid. *Science* **278**, 1937-1940.

Bläßle, A., Soh, G., Braun, T., Morsdorf, D., Preiss, H., Jordan, B. M. and Muller, P. (2018). Quantitative diffusion measurements using the open-source software PyFRAP. *Nature communications* **9**, 1582.

Blumenthal, D., Goldstien, L., Edidin, M. and Gheber, L. A. (2015). Universal Approach to FRAP Analysis of Arbitrary Bleaching Patterns. *Scientific reports* **5**, 11655.

Bobrow, M. N., Harris, T. D., Shaughnessy, K. J. and Litt, G. J. (1989). Catalyzed reporter deposition, a novel method of signal amplification. Application to immunoassays. *Journal of immunological methods* **125**, 279-285.

Bollenbach, T., Kruse, K., Pantazis, P., Gonzalez-Gaitan, M. and Julicher, F. (2007). Morphogen transport in epithelia. *Physical review. E, Statistical, nonlinear, and soft matter physics* **75**, 011901.

Brenner, S. (2002). Life sentences: Detective Rummage investigates. *Genome Biol* **3**, comment1013.1011-comment1013.1012.

Briscoe, J., Chen, Y., Jessell, T. M. and Struhl, G. (2001). A hedgehog-insensitive form of patched provides evidence for direct long-range morphogen activity of sonic hedgehog in the neural tube. *Molecular cell* **7**, 1279-1291.

Briscoe, J. and Small, S. (2015). Morphogen rules: design principles of gradient-mediated embryo patterning. *Development* **142**, 3996-4009.

Brown, J. K., Pemberton, A. D., Wright, S. H. and Miller, H. R. (2004). Primary antibody-Fab fragment complexes: a flexible alternative to traditional direct and indirect immunolabeling techniques. *The journal of histochemistry and cytochemistry : official journal of the Histochemistry Society* **52**, 1219-1230.

Bruce, D. L. and Sapkota, G. P. (2012). Phosphatases in SMAD regulation. *FEBS letters* **586**, 1897-1905.

Burz, D. S. and Hanes, S. D. (2001). Isolation of mutations that disrupt cooperative DNA binding by the Drosophila bicoid protein. *Journal of molecular biology* **305**, 219-230.

Chen, Y. and Schier, A. F. (2001). The zebrafish Nodal signal Squint functions as a morphogen. *Nature* **411**, 607-610.

Ciruna, B., Weidinger, G., Knaut, H., Thisse, B., Thisse, C., Raz, E. and Schier, A. F. (2002). Production of maternal-zygotic mutant zebrafish by germ-line replacement. *Proceedings of the National Academy of Sciences of the United States of America* **99**, 14919-14924.

Cohen, M., Briscoe, J. and Blassberg, R. (2013). Morphogen interpretation: the transcriptional logic of neural tube patterning. *Current opinion in genetics & development* **23**, 423-428.

Crick, F. (1970). Diffusion in embryogenesis. *Nature* **225**, 420-422.

de Olivera-Melo, M., Xu, P. F., Houssin, N., Thisse, B. and Thisse, C. (2018). Generation of ectopic morphogen gradients in the zebrafish blastula. *Methods in molecular biology* **1863**, 125-141.

Dertinger, T., Pacheco, V., von der Hocht, I., Hartmann, R., Gregor, I. and Enderlein, J. (2007). Two-focus fluorescence correlation spectroscopy: a new tool for accurate and absolute diffusion measurements. *Chemphyschem : a European journal of chemical physics and physical chemistry* **8**, 433-443.

Dickmeis, T., Rastegar, S., Aanstad, P., Clark, M., Fischer, N., Korzh, V. and Strähle, U. (2001). Expression of the anti-dorsalizing morphogenetic protein gene in the zebrafish embryo. *Development genes and evolution* **211**, 568-572.

Doyon, Y., McCammon, J. M., Miller, J. C., Faraji, F., Ngo, C., Katibah, G. E., Amora, R., Hocking, T. D., Zhang, L., Rebar, E. J., et al. (2008). Heritable targeted gene disruption in zebrafish using designed zinc-finger nucleases. *Nature biotechnology* **26**, 702-708.

Driever, W. and Nüsslein-Volhard, C. (1988). The bicoid protein determines position in the Drosophila embryo in a concentration-dependent manner. *Cell* **54**, 95-104.

Dubrulle, J., Jordan, B. M., Akhmetova, L., Farrell, J. A., Kim, S. H., Solnica-Krezel, L. and Schier, A. F. (2015). Response to Nodal morphogen gradient is determined by the kinetics of target gene induction. *eLife* **4**, e05042.

Ducy, P. and Karsenty, G. (2000). The family of bone morphogenetic proteins. *Kidney international* **57**, 2207-2214.

Dyson, S. and Gurdon, J. B. (1998). The interpretation of position in a morphogen gradient as revealed by occupancy of activin receptors. *Cell* **93**, 557-568.

Erter, C. E., Solnica-Krezel, L. and Wright, C. V. (1998). Zebrafish nodal-related 2 encodes an early mesendodermal inducer signaling from the extraembryonic yolk syncytial layer. *Developmental biology* **204**, 361-372.

Fauny, J. D., Thisse, B. and Thisse, C. (2009). The entire zebrafish blastula-gastrula margin acts as an organizer dependent on the ratio of Nodal to BMP activity. *Development* **136**, 3811-3819.

Feldman, B., Gates, M. A., Egan, E. S., Dougan, S. T., Rennebeck, G., Sirotkin, H. I., Schier, A. F. and Talbot, W. S. (1998). Zebrafish organizer development and germ-layer formation require nodal-related signals. *Nature* **395**, 181-185.

Ferguson, E. L. and Anderson, K. V. (1992). Decapentaplegic acts as a morphogen to organize dorsal-ventral pattern in the Drosophila embryo. *Cell* **71**, 451-461.

Fisher, S. and Halpern, M. E. (1999). Patterning the zebrafish axial skeleton requires early chordin function. *Nat Genet* **23**, 442-446.

François, P., Vonica, A., Brivanlou, A. H. and Siggia, E. D. (2009). Scaling of BMP gradients in Xenopus embryos. *Nature* **461**, E1; discussion E2.

Gelbart, W. M. (1989). The decapentaplegic gene: a TGF-beta homologue controlling pattern formation in Drosophila. *Development* **107 Suppl**, 65-74.

Green, J. B., New, H. V. and Smith, J. C. (1992). Responses of embryonic Xenopus cells to activin and FGF are separated by multiple dose thresholds and correspond to distinct axes of the mesoderm. *Cell* **71**, 731-739.

Green, J. B. and Smith, J. C. (1990). Graded changes in dose of a Xenopus activin A homologue elicit stepwise transitions in embryonic cell fate. *Nature* **347**, 391-394.

Gritsman, K., Zhang, J., Cheng, S., Heckscher, E., Talbot, W. S. and Schier, A. F. (1999). The EGF-CFC protein one-eyed pinhead is essential for nodal signaling. *Cell* **97**, 121-132.

Gurdon, J. B., Harger, P., Mitchell, A. and Lemaire, P. (1994). Activin signalling and response to a morphogen gradient. *Nature* **371**, 487-492.

Gurdon, J. B., Mitchell, A. and Mahony, D. (1995). Direct and continuous assessment by cells of their position in a morphogen gradient. *Nature* **376**, 520-521.

Hans, S., Christison, J., Liu, D. and Westerfield, M. (2007). Fgf-dependent otic induction requires competence provided by Foxi1 and Dlx3b. *BMC developmental biology* **7**, 5.

Harmansa, S., Alborelli, I., Bieli, D., Caussinus, E. and Affolter, M. (2017). A nanobody-based toolset to investigate the role of protein localization and dispersal in Drosophila. *eLife* **6**, e22549.

Heldin, C. H., Miyazono, K. and ten Dijke, P. (1997). TGF-β signalling from cell membrane to nucleus through SMAD proteins. *Nature* **390**, 465-471.

Hild, M., Dick, A., Rauch, G. J., Meier, A., Bouwmeester, T., Haffter, P. and Hammerschmidt, M. (1999). The smad5 mutation somitabun blocks Bmp2b signaling during early dorsoventral patterning of the zebrafish embryo. *Development* **126**, 2149-2159.

Holley, S. A., Neul, J. L., Attisano, L., Wrana, J. L., Sasai, Y., O'Connor, M. B., De Robertis, E. M. and Ferguson, E. L. (1996). The Xenopus dorsalizing factor noggin ventralizes Drosophila embryos by preventing DPP from activating its receptor. *Cell* **86**, 607-617.

Howard, M. and ten Wolde, P. R. (2005). Finding the center reliably: robust patterns of developmental gene expression. *Physical review letters* **95**, 208103.

Hruscha, A., Krawitz, P., Rechenberg, A., Heinrich, V., Hecht, J., Haass, C. and Schmid, B. (2013). Efficient CRISPR/Cas9 genome editing with low off-target effects in zebrafish. *Development* **140**, 4982-4987.

Huisken, J., Swoger, J., Del Bene, F., Wittbrodt, J. and Stelzer, E. H. (2004). Optical sectioning deep inside live embryos by selective plane illumination microscopy. *Science* **305**, 1007-1009.

Inomata, H., Shibata, T., Haraguchi, T. and Sasai, Y. (2013). Scaling of dorsal-ventral patterning by embryo size-dependent degradation of Spemann's organizer signals. *Cell* **153**, 1296-1311.

Joly, J. S., Joly, C., Schulte-Merker, S., Boulekbache, H. and Condamine, H. (1993). The ventral and posterior expression of the zebrafish homeobox gene eve1 is perturbed in dorsalized and mutant embryos. *Development* **119**, 1261-1275.

Jullien, J. and Gurdon, J. (2005). Morphogen gradient interpretation by a regulated trafficking step during ligand-receptor transduction. *Genes & development* **19**, 2682-2694.

Kerszberg, M. and Wolpert, L. (2007). Specifying positional information in the embryo: looking beyond morphogens. *Cell* **130**, 205-209.

Lecuit, T., Brook, W. J., Ng, M., Calleja, M., Sun, H. and Cohen, S. M. (1996). Two distinct mechanisms for long-range patterning by Decapentaplegic in the Drosophila wing. *Nature* **381**, 387-393.

Lele, Z., Nowak, M. and Hammerschmidt, M. (2001). Zebrafish admp is required to restrict the size of the organizer and to promote posterior and ventral development. *Developmental dynamics : an official publication of the American Association of Anatomists* **222**, 681-687.

Liebman, P. A. and Entine, G. (1974). Lateral diffusion of visual pigment in photorecptor disk membranes. *Science* **185**, 457-459.

Little, S. C. and Mullins, M. C. (2009). Bone morphogenetic protein heterodimers assemble heteromeric type I receptor complexes to pattern the dorsoventral axis. *Nature cell biology* **11**, 637-643.

Marois, E., Mahmoud, A. and Eaton, S. (2006). The endocytic pathway and formation of the Wingless morphogen gradient. *Development* **133**, 307-317.

Mathieu, J., Griffin, K., Herbomel, P., Dickmeis, T., Strahle, U., Kimelman, D., Rosa, F. M. and Peyrieras, N. (2004). Nodal and Fgf pathways interact through a positive regulatory loop and synergize to maintain mesodermal cell populations. *Development* **131**, 629-641.

McHale, P., Rappel, W. J. and Levine, H. (2006). Embryonic pattern scaling achieved by oppositely directed morphogen gradients. *Physical biology* **3**, 107-120.

Meno, C., Gritsman, K., Ohishi, S., Ohfuji, Y., Heckscher, E., Mochida, K., Shimono, A., Kondoh, H., Talbot, W. S., Robertson, E. J., et al. (1999). Mouse Lefty2 and zebrafish antivin are feedback inhibitors of nodal signaling during vertebrate gastrulation. *Molecular cell* **4**, 287-298.

Michaelis, L., Menten, M. L., Johnson, K. A. and Goody, R. S. (2011). The original Michaelis constant: translation of the 1913 Michaelis-Menten paper. *Biochemistry* **50**, 8264-8269.

Miller-Bertoglio, V. E., Fisher, S., Sanchez, A., Mullins, M. C. and Halpern, M. E. (1997). Differential regulation of chordin expression domains in mutant zebrafish. *Developmental biology* **192**, 537-550.

Mizutani, C. M., Nie, Q., Wan, F. Y., Zhang, Y. T., Vilmos, P., Sousa-Neves, R., Bier, E., Marsh, J. L. and Lander, A. D. (2005). Formation of the BMP activity gradient in the Drosophila embryo. *Developmental cell* **8**, 915-924.

Montague, T. G. and Schier, A. F. (2017). Vg1-Nodal heterodimers are the endogenous inducers of mesendoderm. *eLife* **6**, e28183.

Mörsdorf, D. and Müller, P. (2019). Tuning protein diffusivity with membrane tethers. *Biochemistry* **58**, 177-181.

Müller, P., Rogers, K. W., Jordan, B. M., Lee, J. S., Robson, D., Ramanathan, S. and Schier, A. F. (2012). Differential diffusivity of Nodal and Lefty underlies a reaction-diffusion patterning system. *Science* **336**, 721-724.

Müller, P., Rogers, K. W., Yu, S. R., Brand, M. and Schier, A. F. (2013). Morphogen transport. *Development* **140**, 1621-1638.

Muraoka, O., Shimizu, T., Yabe, T., Nojima, H., Bae, Y. K., Hashimoto, H. and Hibi, M. (2006). Sizzled controls dorso-ventral polarity by repressing cleavage of the Chordin protein. *Nature cell biology* **8**, 329-338.

Nellen, D., Burke, R., Struhl, G. and Basler, K. (1996). Direct and long-range action of a DPP morphogen gradient. *Cell* **85**, 357-368.

Niessing, D., Blanke, S. and Jäckle, H. (2002). Bicoid associates with the 5'-cap-bound complex of caudal mRNA and represses translation. *Genes & development* **16**, 2576-2582.

Padgett, R. W., St Johnston, R. D. and Gelbart, W. M. (1987). A transcript from a Drosophila pattern gene predicts a protein homologous to the transforming growth factor-beta family. *Nature* **325**, 81-84.

Pelliccia, J. L., Jindal, G. A. and Burdine, R. D. (2017). Gdf3 is required for robust Nodal signaling during germ layer formation and left-right patterning. *eLife* **6**, e28635.

Pogoda, H. M. and Meyer, D. (2002). Zebrafish Smad7 is regulated by Smad3 and BMP signals. *Developmental dynamics : an official publication of the American Association of Anatomists* **224**, 334-349.

Pomreinke, A. P., Soh, G. H., Rogers, K. W., Bergmann, J. K., Bläßle, A. J. and Müller, P. (2017). Dynamics of BMP signaling and distribution during zebrafish dorsal-ventral patterning. *eLife* **6**, 25861.

Poo, M. and Cone, R. A. (1973). Lateral diffusion of rhodopsin in the visual receptor membrane. *Journal of supramolecular structure* **1**, 354.

Poulain, M., Furthauer, M., Thisse, B., Thisse, C. and Lepage, T. (2006). Zebrafish endoderm formation is regulated by combinatorial Nodal, FGF and BMP signalling. *Development* **133**, 2189-2200.

Preibisch, S., Saalfeld, S., Schindelin, J. and Tomancak, P. (2010). Software for bead-based registration of selective plane illumination microscopy data. *Nature methods* **7**, 418-419.

Ramel, M. C., Buckles, G. R., Baker, K. D. and Lekven, A. C. (2005). WNT8 and BMP2B co-regulate non-axial mesoderm patterning during zebrafish gastrulation. *Developmental biology* **287**, 237-248.

Ramel, M. C. and Hill, C. S. (2013). The ventral to dorsal BMP activity gradient in the early zebrafish embryo is determined by graded expression of BMP ligands. *Developmental biology* **378**, 170-182.

Ramel, M. C. and Lekven, A. C. (2004). Repression of the vertebrate organizer by Wnt8 is mediated by Vent and Vox. *Development* **131**, 3991-4000.

Ramirez-Weber, F. A. and Kornberg, T. B. (1999). Cytonemes: cellular processes that project to the principal signaling center in Drosophila imaginal discs. *Cell* **97**, 599-607.

Rapsomaniki, M. A., Kotsantis, P., Symeonidou, I. E., Giakoumakis, N. N., Taraviras, S. and Lygerou, Z. (2012). easyFRAP: an interactive, easy-to-use tool for qualitative and quantitative analysis of FRAP data. *Bioinformatics* **28**, 1800-1801.

Rebagliati, M. R., Toyama, R., Haffter, P. and Dawid, I. B. (1998). cyclops encodes a nodal-related factor involved in midline signaling. *Proceedings of the National Academy of Sciences of the United States of America* **95**, 9932-9937.

Rodaway, A., Takeda, H., Koshida, S., Broadbent, J., Price, B., Smith, J. C., Patient, R. and Holder, N. (1999). Induction of the mesendoderm in the zebrafish germ ring by yolk cell-derived TGF-β family signals and discrimination of mesoderm and endoderm by FGF. *Development* **126**, 3067-3078.

Rogers, K. W., Bläßle, A., Schier, A. F. and Müller, P. (2015). Measuring protein stability in living zebrafish embryos using fluorescence decay after photoconversion (FDAP). *Journal of visualized experiments : JoVE* **95**, 52266.

Rogers, K. W., Lord, N. D., Gagnon, J. A., Pauli, A., Zimmerman, S., Aksel, D., Reyon, D., Tsai, S. Q., Joung, J. K. and Schier, A. F. (2017). Nodal patterning without Lefty inhibitory feedback is functional but fragile. *eLife* **6**, 28785.

Rogers, K. W. and Müller, P. (2019). Nodal and BMP dispersal during early zebrafish development. *Developmental biology* **447**, 14-23.

Rogers, K. W. and Schier, A. F. (2011). Morphogen gradients: from generation to interpretation. *Annual review of cell and developmental biology* **27**, 377-407.

Sampath, K., Rubinstein, A. L., Cheng, A. M., Liang, J. O., Fekany, K., Solnica-Krezel, L., Korzh, V., Halpern, M. E. and Wright, C. V. (1998). Induction of the zebrafish ventral brain and floorplate requires cyclops/nodal signalling. *Nature* **395**, 185-189.

Schaff, J. C., Cowan, A. E., Loew, L. M. and Moraru, I. I. (2009). Virtual FRAP - an Experiment-Oriented Simulation Tool. *Biophysical journal* **96**, 30a-30a.

Schmid, B., Fürthauer, M., Connors, S. A., Trout, J., Thisse, B., Thisse, C. and Mullins, M. C. (2000). Equivalent genetic roles for bmp7/snailhouse and bmp2b/swirl in dorsoventral pattern formation. *Development* **127**, 957-967.

Schmid, B., Shah, G., Scherf, N., Weber, M., Thierbach, K., Campos, C. P., Roeder, I., Aanstad, P. and Huisken, J. (2013). High-speed panoramic light-sheet microscopy reveals global endodermal cell dynamics. *Nature communications* **4**, 2207.

Scholpp, S. and Brand, M. (2004). Endocytosis controls spreading and effective signaling range of Fgf8 protein. *Current biology : CB* **14**, 1834-1841.

Schulte-Merker, S., Lee, K. J., McMahon, A. P. and Hammerschmidt, M. (1997). The zebrafish organizer requires chordino. *Nature* **387**, 862-863.

Shen, M. M. and Schier, A. F. (2000). The EGF-CFC gene family in vertebrate development. *Trends in genetics : TIG* **16**, 303-309.

Spemann, H. and Mangold, H. (1924). Über Induktion von Embryonalanlagen durch Implantation artfremder Organisatoren. *Arch. mikrok. Anat. u. Entw.mechan.* **100**, 599-638.

Takahashi, K. and Yamanaka, S. (2006). Induction of pluripotent stem cells from mouse embryonic and adult fibroblast cultures by defined factors. *Cell* **126**, 663-676.

Teleman, A. A. and Cohen, S. M. (2000). Dpp gradient formation in the Drosophila wing imaginal disc. *Cell* **103**, 971-980.

Toth, Z. E. and Mezey, E. (2007). Simultaneous visualization of multiple antigens with tyramide signal amplification using antibodies from the same species. *The journal of histochemistry and cytochemistry : official journal of the Histochemistry Society* **55**, 545-554.

Tsang, M., Kim, R., de Caestecker, M. P., Kudoh, T., Roberts, A. B. and Dawid, I. B. (2000). Zebrafish nma is involved in TGFβ family signaling. *Genesis* **28**, 47-57.

Turing, A. M. (1952). The Chemical Basis of Morphogenesis. *Philosophical transactions of the Royal Society of London. Series B, Biological sciences* **237**, 37-72.

Urist, M. R. (1965). Bone: formation by autoinduction. *Science* **150**, 893-899.

van Boxtel, A. L., Chesebro, J. E., Heliot, C., Ramel, M. C., Stone, R. K. and Hill, C. S. (2015). A temporal window for signal activation dictates the dimensions of a Nodal signaling domain. *Developmental cell* **35**, 175-185.

van Boxtel, A. L., Economou, A. D., Heliot, C. and Hill, C. S. (2018). Long-range signaling activation and local inhibition separate the mesoderm and endoderm lineages. *Developmental cell* **44**, 179-191 e175.

Wang, Y. C. and Ferguson, E. L. (2005). Spatial bistability of Dpp-receptor interactions during Drosophila dorsal-ventral patterning. *Nature* **434**, 229-234.

Westerfield, M. (1993). *The zebrafish book : a guide for the laboratory use of zebrafish (Brachydanio rerio)*. Eugene, OR: M. Westerfield.

Willot, V., Mathieu, J., Lu, Y., Schmid, B., Sidi, S., Yan, Y. L., Postlethwait, J. H., Mullins, M., Rosa, F. and Peyrieras, N. (2002). Cooperative action of ADMP- and BMP-mediated pathways in regulating cell fates in the zebrafish gastrula. *Developmental biology* **241**, 59-78.

Wolpert, L. (1969). Positional information and the spatial pattern of cellular differentiation. *J Theor Biol* **25**, 1-47.

Wozney, J. M., Rosen, V., Celeste, A. J., Mitsock, L. M., Whitters, M. J., Kriz, R. W., Hewick, R. M. and Wang, E. A. (1988). Novel regulators of bone formation: molecular clones and activities. *Science* **242**, 1528-1534.

Wrana, J. L., Attisano, L., Carcamo, J., Zentella, A., Doody, J., Laiho, M., Wang, X. F. and Massague, J. (1992). TGFβ signals through a heteromeric protein kinase receptor complex. *Cell* **71**, 1003-1014.

Xu, P. F., Houssin, N., Ferri-Lagneau, K. F., Thisse, B. and Thisse, C. (2014). Construction of a vertebrate embryo from two opposing morphogen gradients. *Science* **344**, 87-89.

Xue, Y., Zheng, X., Huang, L., Xu, P., Ma, Y., Min, Z., Tao, Q., Tao, Y. and Meng, A. (2014). Organizer-derived Bmp2 is required for the formation of a correct Bmp activity gradient during embryonic development. *Nature communications* **5**, 3766.

Yan, Y., Ning, G., Li, L., Liu, J., Yang, S., Cao, Y. and Wang, Q. (2019). The BMP ligand Pinhead together with Admp supports the robustness of embryonic patterning. *Science advances* **5**, eaau6455.

Yoney, A., Etoc, F., Ruzo, A., Carroll, T., Metzger, J. J., Martyn, I., Li, S., Kirst, C., Siggia, E. D. and Brivanlou, A. H. (2018). WNT signaling memory is required for ACTIVIN to function as a morphogen in human gastruloids. *eLife* **7**, e38279.

Yu, S. R., Burkhardt, M., Nowak, M., Ries, J., Petrasek, Z., Scholpp, S., Schwille, P. and Brand, M. (2009). Fgf8 morphogen gradient forms by a source-sink mechanism with freely diffusing molecules. *Nature* **461**, 533-536.

Zhou, X., Sasaki, H., Lowe, L., Hogan, B. L. and Kuehn, M. R. (1993). Nodal is a novel TGF-β-like gene expressed in the mouse node during gastrulation. *Nature* **361**, 543-547.

Zinski, J., Bu, Y., Wang, X., Dou, W., Umulis, D. and Mullins, M. (2017). Systems biology derived source-sink mechanism of BMP gradient formation. *eLife* **6**, e22199.

Zu, Y., Tong, X., Wang, Z., Liu, D., Pan, R., Li, Z., Hu, Y., Luo, Z., Huang, P., Wu, Q., et al. (2013). TALEN-mediated precise genome modification by homologous recombination in zebrafish. *Nature methods* **10**, 329-331.

8. Appendix

Publications

1. **Pomreinke, A. P., Soh, G. H., Rogers, K. W., Bergmann, J. K., Bläßle, A. J. and Müller, P.** (2017). Dynamics of BMP signaling and distribution during zebrafish dorsal-ventral patterning. *eLife* **6**, 25861. https://pubmed.ncbi.nlm.nih.gov/28857744/

2. **Bläßle, A., Soh, G., Braun, T., Morsdorf, D., Preiss, H., Jordan, B. M. and Muller, P.** (2018). Quantitative diffusion measurements using the open-source software PyFRAP. *Nature communications* **9**, 1582. https://pubmed.ncbi.nlm.nih.gov/29679054/

3. **Soh, G. H., Müller, P.** (2018). FRAP analysis of Extracellular Diffusion in Zebrafish Embryos. *Methods in Molecular Biology* **1863**, 107-124. https://pubmed.ncbi.nlm.nih.gov/30324594/

4. **Almuedo-Castillo, M., Bläßle, A., Mörsdorf, D., Marcon, L., Soh, G. H., Rogers, K. W., Schier, A. F. and Müller, P.** (2018). Scale-invariant patterning by size-dependent inhibition of Nodal signalling. *Nature cell biology* **20**, 1032-1042. https://pubmed.ncbi.nlm.nih.gov/30061678/

5. **Soh, G. H., Pomreinke, A. P., Müller, P.** (2020). Integration of Nodal and BMP signaling by mutual signaling effector antagonism. *Cell Reports* **31**, 107487. https://pubmed.ncbi.nlm.nih.gov/32268105/